NATIONAL AERONAUTICS AND SPACE ADMINISTRATION

Technical Memorandum 33-708

Jupiter's Radiation Belts and Their Effects on Spacecraft

Richard H. Parker
Edward L. Divita
Gunter Gigas

JET PROPULSION LABORATORY
CALIFORNIA INSTITUTE OF TECHNOLOGY
PASADENA, CALIFORNIA

October 15, 1974

NATIONAL AERONAUTICS AND SPACE ADMINISTRATION

Technical Memorandum 33-708

Jupiter's Radiation Belts and Their Effects on Spacecraft

Richard H. Parker
Edward L. Divita
Gunter Gigas

JET PROPULSION LABORATORY
CALIFORNIA INSTITUTE OF TECHNOLOGY
PASADENA, CALIFORNIA

October 15, 1974

PREFACE

The work described in this report was performed by the Space Sciences and Project Engineering Divisions of the Jet Propulsion Laboratory, under the cognizance of the Mariner Jupiter/Saturn 1977 Project.

FOREWORD

This report contains the earliest formal description of the Jupiter Radiation Belt Model prepared from Pioneer 10 observations. A more recent updated model, following the publication of detailed observations in the Journal of Geophysical Research, is currently being used. In particular, the new model to be used by the MJS77 Project will be published soon as a JPL Technical Memorandum.

ACKNOWLEDGMENT

This memorandum was originally prepared as a paper which was presented at the International Conference on Evaluation of Space Environment on Materials held in Toulouse, France, on June 17 - 21, 1974. The work reported includes some results of radiation studies, tests and observations performed over the past several years by numerous scientists and engineers.

In particular, several individuals require specific acknowledgment. Jupiter radiation models both pre- and post-Pioneer 10 encounter, used extensively, were generally based on studies and work of T. N. Divine of the Jet Propulsion Laboratory. K. E. Martin and D. Bergens, of the Jet Propulsion Laboratory, provided a large amount of their detailed test data on the selected sensitive piece-parts which led us to several well-supported major conclusions.

The authors wish to extend a general acknowledgment to all those contributing individuals not specifically identified.

Special thanks are due M. F. Buehler, technical editor, for her unfailing help in providing a continuity in style.

We gratefully acknowledge the support of the Thermoelectric Outer Planets Spacecraft Study and the Mariner Jupiter/Saturn 1977 Project.

CONTENTS

TABLES

FIGURES

ABSTRACT

The effects of electron and proton radiation on spacecraft which will operate in the trapped radiation belts of the planet Jupiter are considered, and the techniques and results of the testing and simulation used in the radiation effects program at the Jet Propulsion Laboratory (JPL) are discussed. Available data from the Pioneer 10 encounter of Jupiter are compared with pre-encounter models of the Jupiter radiation belts. The implications that the measured Jovian radiation belts have for future missions are considered.

I. INTRODUCTION

Since 1968, NASA/JPL has studied the effects of charged particles, trapped near the planet Jupiter, on the performance of a Mariner class spacecraft. The evolution of radiation models of Jupiter's trapped radiation belts resulted in analyses and tests which covered a large range of charged particle effects. However, the Jovian radiation levels recently observed by Pioneer 10 are higher than expected and provide a challenging environment for NASA's interplanetary missions. The Mariner Jupiter/Saturn 1977 (MJS77) will be the first Mariner class spacecraft to be subjected to Jupiter's radiation belts. Although not considered in this paper, the radiation environment for MJS77 includes a contribution from the on-board electrical power provided by Radioisotopic Thermoelectric Generators (RTG) which emit neutron and gamma radiation. Thus radiation analyses and tests representing many major radiation types have been and are being performed at JPL under this project and its precursor programs.

The MJS77 approach is to isolate and to replace the most radiation-susceptible parts, materials and circuit designs until the spacecraft is "hard" enough to withstand the anticipated radiation environment. The radiation exposures can be controlled to a degree by the trajectory selection in terms of closeness of approach to Jupiter. Inherent spacecraft shielding and, if necessary, small amounts of additional shielding will be utilized. This is a cost effective method to harden a spacecraft, which is partly designed through using inherited hardware for which high levels of radiation were not originally considered.

This paper considers the Jovian radiation environment, the effects of radiation, and the prediction of their effects on spacecraft operating in the vicinity of Jupiter. Data on radiation effects from laboratory tests and Pioneer 10 flyby measurements have been used. Section II considers the evolution of models for the Jovian belts; selected models are briefly described. The latest model is based on preliminary data from the December 4, 1973, Jupiter encounter by Pioneer 10. Fluxes and fluences (for particular MJS77 trajectories) and the energy spectra are presented. In the third section, a discussion on simulation techniques is given including (i) energy equivalencing for electrons and protons, (ii) accelerated flux testing, and (iii) damage correlation between particle types.

In the fourth and fifth sections, data on irradiation of spacecraft piece parts and materials using proton and electron sources respectively are discussed. These sections specifically discuss selected radiation-sensitive piece-parts and ience devices.

In the final section, predictions of the effects of radiation on the MJS77 spacecraft and the approaches being taken to assure a successful mission are discussed.

A. Radio Astronomy Observations of Jupiter

From 1958 through 1962, many observers noted a strong nonthermal radiation in the decimetric wavelengths around Jupiter (Refs. 1 and 2). By 1962, most scientists agreed that Jupiter had a radiation belt which produced the observed nonthermal emissions (Ref. 3). The predominant theory postulated synchrotron emission caused by high-energy (MeV) electrons radiating while accelerated in the magnetic field of Jupiter.

In 1966, Berge (Ref. 4) made interferometric observations and constructed a two-dimensional contour map of the brightness temperature corresponding to 10.4-cm radiation in the emitting region by assuming a symmetrical synchrotron emission component. Berge's best fit is shown in Fig. 1.

In 1968, Branson (Ref. 5) prepared brightness contour maps corresponding to 21-cm radiation for each of three central meridian longitudes (System III-1957.0), separated by 120 deg, using an aperture-synthesis process. Fig. 2 shows the three maps. The contours indicate a magnetic moment tilt and an asymmetry in the emissions. Both Berge's and Branson's measurements strongly support the mechanism of synchrotron emission by electrons.

Further measurements indicate a rotation period of 9 h 55 m 29.73 s ±0.26 s, which is nearly equal to the System III-1957 period (i.e., 0.46 s longer). Thus, the trapped electron belt theory was well established with a broad intensity maximum near 1.8 R_J ($R_J \equiv$ Jupiter radius = (7.14 ± 0.02) × 10^4 km measured from the jovigraphic center of the planet).

Trapped Jovian protons were not expected to be observable by radio emissions since their predicted wavelengths would be longer and in the thermal background. The possibility of the decimetric emissions being caused by trapped protons was discarded because of the excessively large magnetic fields and proton energies required.

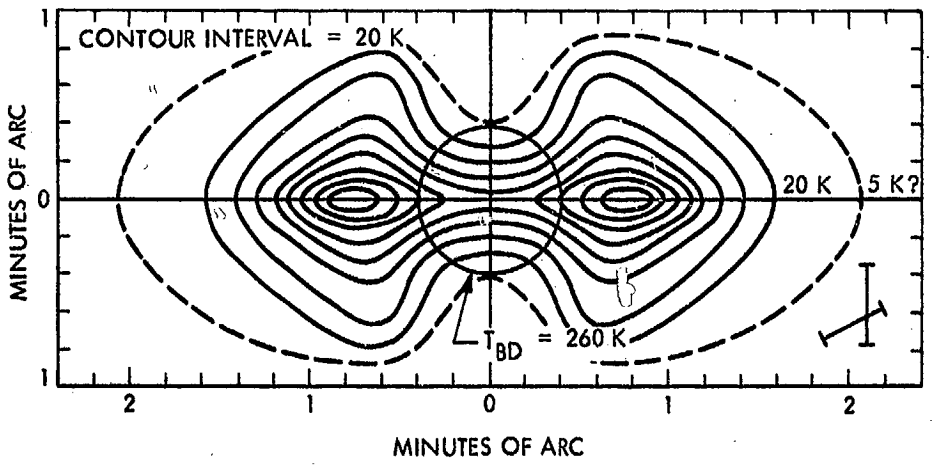

Fig. 1. Aperture synthesis map of Jupiter's 10.4-cm radiation. The central circle represents Jupiter's optical disk, the curved lines represent contours of constant brightness temperature, and the bars at lower right indicate the instrumental resolution (from Ref. 4)

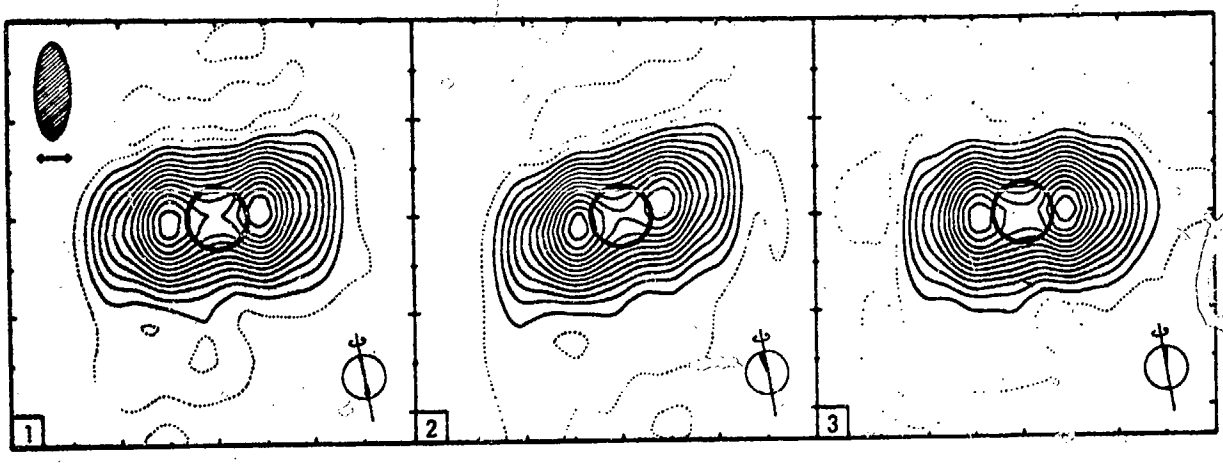

Fig. 2. Three aperture synthesis maps of Jupiter's 21-cm radiation. The central circles represent Jupiter's optical disk, the curved lines represent contours of constant brightness temperature (interval 47 K), the oval at upper left represents the instrumental resolution, and the figures at lower right represent the orientations of the rotational and magnetic axes (from Ref. 5)

B. Early Belt Models

Many attempts have been made to construct models using the brightness contours and earth analogies, as shown in Fig. 3. Warwick (Ref. 6) developed a consistent L-shell diffusion model, predicting an offset of the dipole moment and a surface equatorial field of 2 gauss. A characteristic energy of 6.2 MeV and a flux of 1.9×10^7 e/cm^2-s were predicted for this electron belt peaking at 1.8 R_J, as shown, along with several other models for comparison (Refs. 7-13). The characteristic energy is the dominant or mode energy of the spectral distribution.

Warwick further developed a proton model by earth analogy which predicted a characteristic proton energy at 1.8 R_J of 29 MeV and a flux of 1.1×10^6 p/cm^2-s, shown in Fig. 4. Divine (Ref. 14) modified Warwick's model slightly as a result of the 1971 Jupiter Radiation Belt Workshop (Ref. 15), in which some 30 scientists, using "democratic, interactive techniques," developed the 1971 Workshop Model. This model, which is also an L-shell diffusion model, has been updated as a 1971 Post-Workshop Model to include relativistic effects and ion-cyclotron instabilities. The electron and proton models from this workshop are shown in Fig. 5. The feature at ~12 R_J for the upper limit proton model is the result of the attempt to consider the ion-cyclotron instability where energetic protons interact with local plasma waves at frequencies near the ion-cyclotron frequency (T. N. Divine in Ref. 15, Appendix B).

During the Thermoelectric Outer Planets Spacecraft (TOPS) study at JPL (Refs. 16, 17), the Warwick and Divine model was used. This model predicted proton fluences as high as 2×10^{13} p/cm^2 (20 MeV equivalent level - see Section III for definition) from the upper limit model on a trajectory with 1.07 R_J periapsis. Other trajectories were considered with periapses out to 12 R_J, where the radiation levels were insignificant since the protons were not energetic enough to penetrate to sensitive regions. Later, with approximately three orders of magnitude difference between the nominal and upper limit protons in the 1971 Workshop Models, a large variety of levels had to be considered for MJS77. The electron environment appeared to be much less hostile than the proton (Ref. 15), particularly

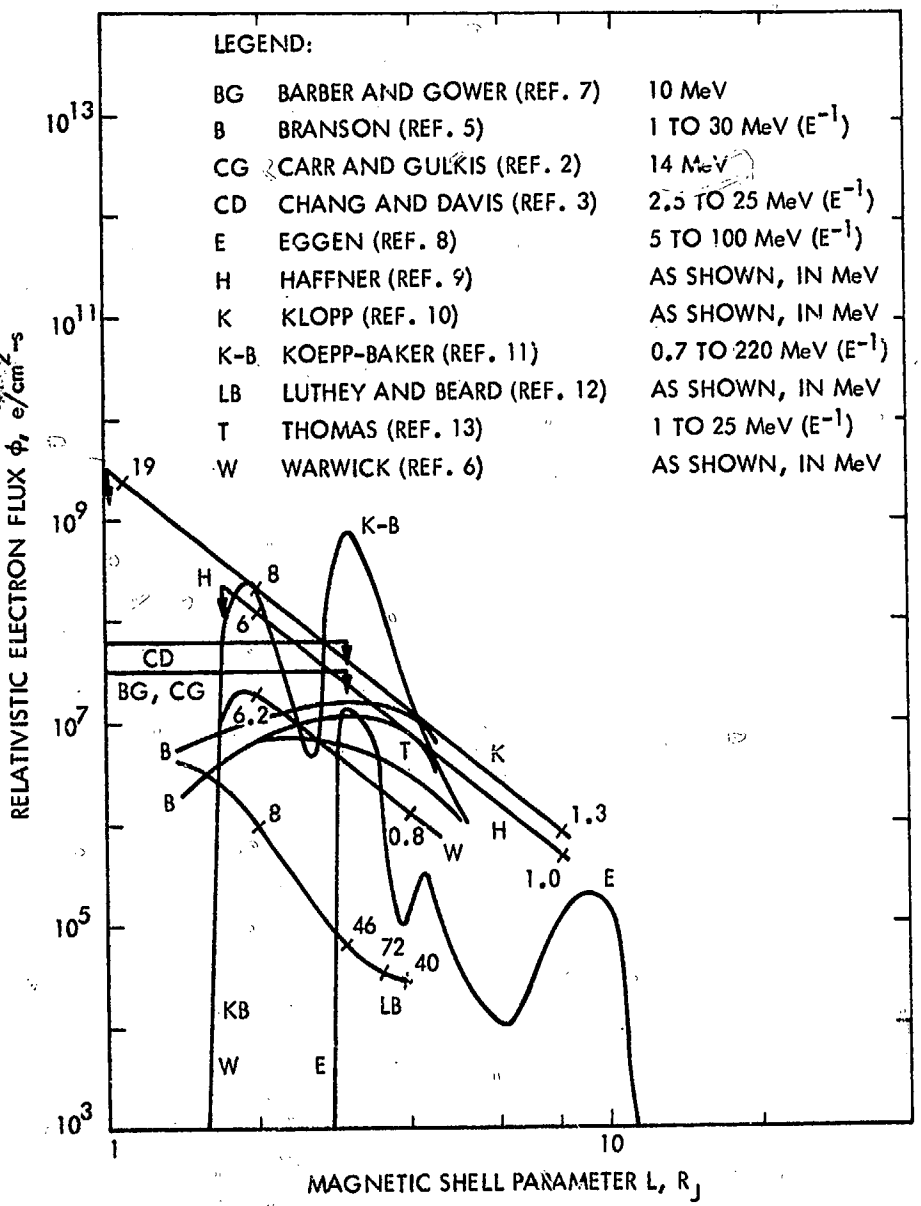

Fig. 3. Jupiter electron models in equatorial plane

since the ratio of displacement damage constants for protons of 20 MeV to electrons of 3 MeV is 5×10^3 (see, for example, Ref. 18).

The 1971 workshop, which was initiated with the hope of solving a difficult radiation problem, created a model which lowered the upper limit electron model and raised the upper limit proton model by nearly two orders of magnitude. The upper limit model even contained protons with energies of 1 to 3×10^9 eV. The high-energy protons were removed in the 1971 Post-Workshop Model (Ref. 15, Appendix B).

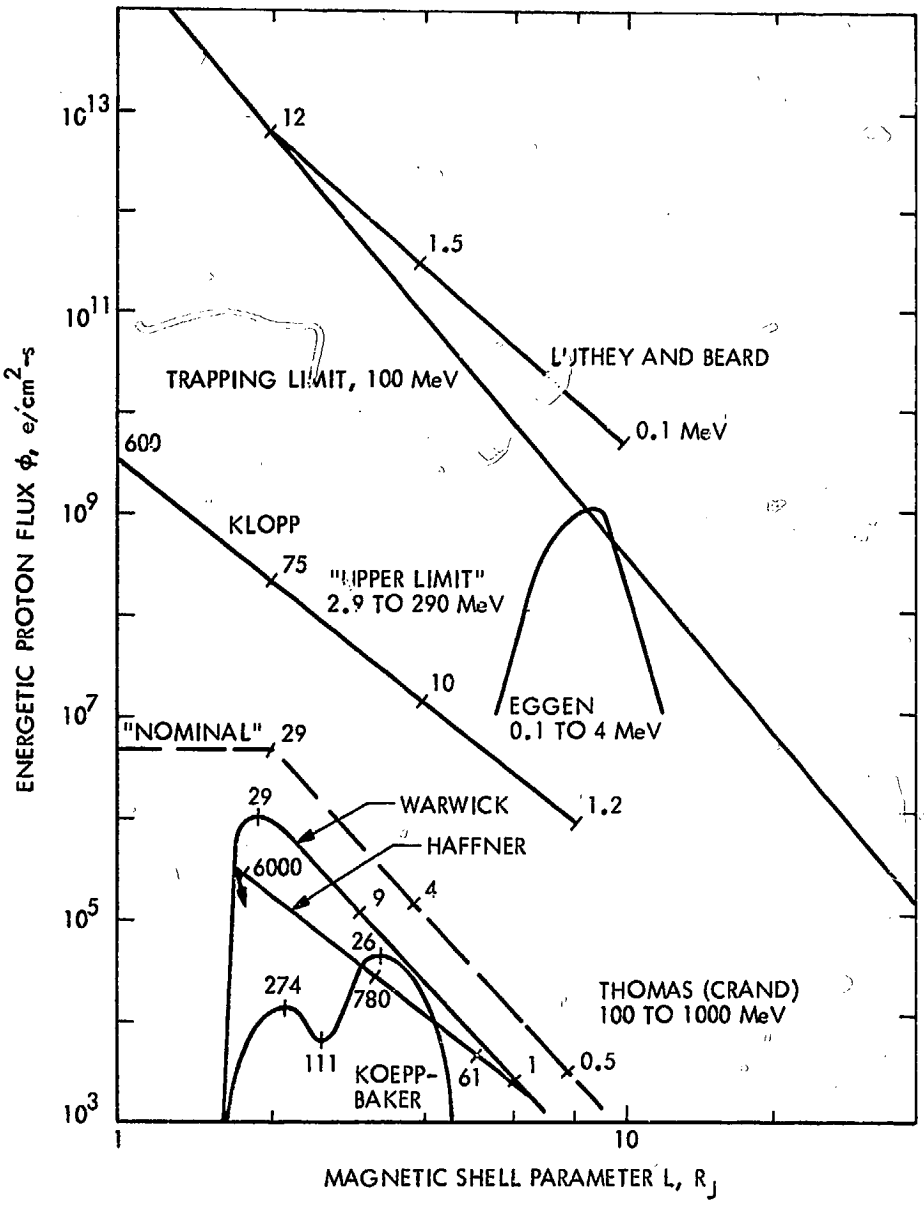

Fig. 4. Jupiter proton models (including the 1971 Workshop Model) in equatorial plane (energies in MeV)

Two additional theoretical models which are different from the usual L-shell diffusion models have been considered. Shawhan et al. (Ref. 19) provided a model which predicted a significant electron source based on a Debye sheath at the Jovian satellite Io large enough to supply the 1971 Workshop model densities for $1 \leq L \leq 2$. Hess, Mead, and colleagues (Ref. 20) proposed in a series of papers that the five inner satellites of Jupiter remove most of the protons in the radiation belts. They pointed out that proton gyroradii are small compared to the satellite diameters. Since bounce times are not long, and in the absence of electric or magnetic deflection around the satellites, protons will impact Io and be lost from the belts. A large number of other predictions relating to the belt fluxes were published prior to the Pioneer 10 encounter, all of which were based on L-shell diffusion.

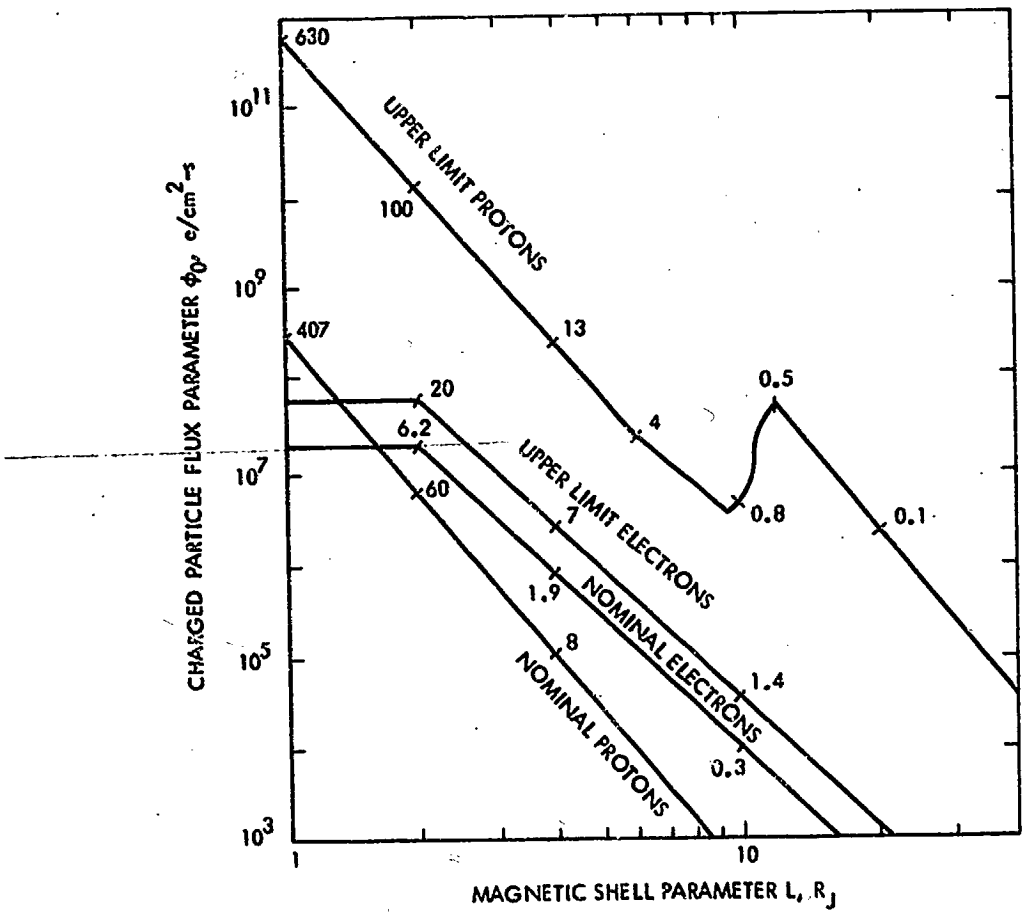

Fig. 5. Fluxes of charged particles in Jupiter's trapped radiation belts, as functions of distance from the magnetic dipole in the magnetic equatorial plane. Local values of the characteristic energy E_o are shown in MeV (1971 Post-Workshop Model)

C. Pioneer 10 Measurements

Preliminary calculations using the electron and proton flux models developed at the recent Pioneer 10 Jupiter Radiation Belt Workshop (held at NASA Ames Research Center, February 19-21, 1974) are compared with preliminary observations in Figs. 6 and 7. The upper two curves in Fig. 6 represent the flux of electrons with energy $E_e > 3$, and $E_e > 21$ MeV along the magnetic equator based on the preliminary data and equations from the 1974 workshop. The discontinuity near L = 6, which may represent the sweeping by Io, is present in the data from the University of Chicago (UC) experiment (Ref. 21). The UC data are taken along the flight path. The University of Iowa (UI) flux data are evaluated from the equation in Ref. 21 for electrons with $E_e > 21$ MeV along the magnetic equator. The lower two curves in the figure represent the upper limit of the 1971 Post-Workshop Electron Model. The characteristic energy at several locations is indicated on curve E. Notice that the actual belt is much more intense and extensive than predicted by the upper limit model.

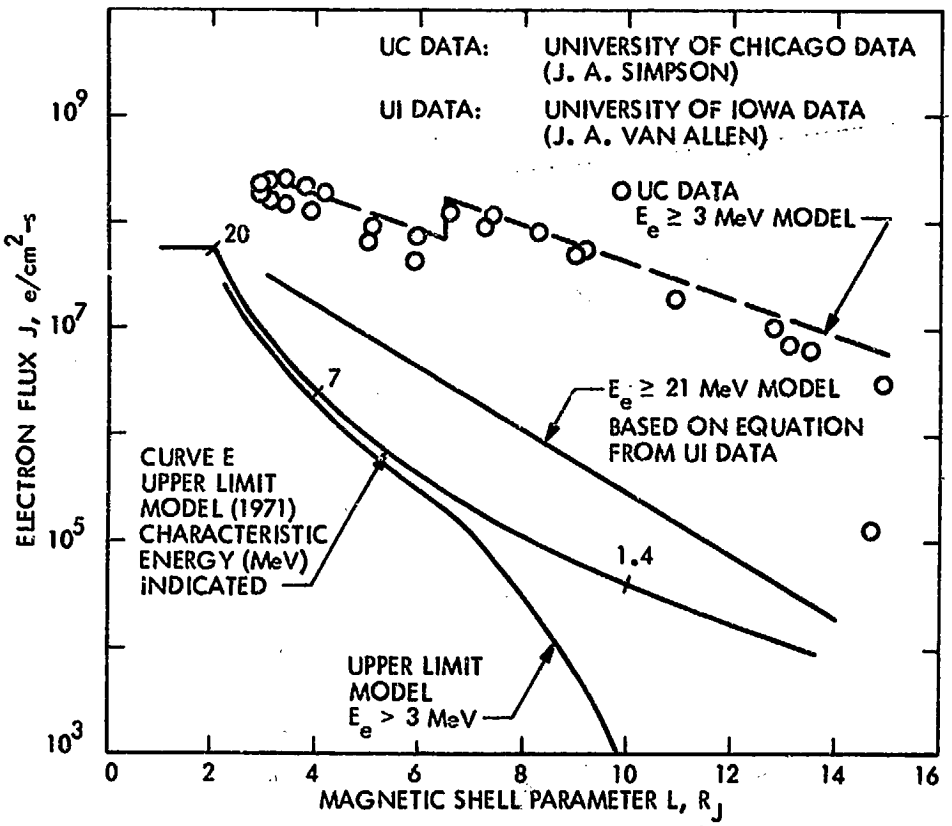

Fig. 6. Pioneer 10 experimental data and preliminary 1974 workshop data for Jupiter-trapped electrons compared with the 1971 Post-Workshop Model

The same comparisons are made in Fig. 7 between the 1971 Workshop Model and some preliminary observations of protons at E >30 and E >70 MeV, taken from University of Chicago and University of California at San Diego data (1974 workshop data and Ref. 21), respectively. Again, the solid lines represent the upper limit of the model derived from the 1971 Workshop. Curve P shows the characteristic energy flux profile. For protons with energy above 30 MeV, note that the measured values for the 1974 model fall below the upper limit model within 6 R_J; but beyond ~6 R_J the measured values are increasingly larger than the fluxes in the upper limit model.

Electron fluxes and energies are now of major concern to Jupiter flyby and orbiting spacecraft designers. The protons, although of some concern to designers (for example, in relation to exposed science optics) are not large enough in energy and fluence to produce significant degradation to internal electronics. This is anticipated because even if the proton low energy contribution proved to be significant, the 0.34 - 0.56 g/cm^2 of aluminum shielding inherent in spacecraft housing and covers would stop protons with energies less than about 15-20 MeV.

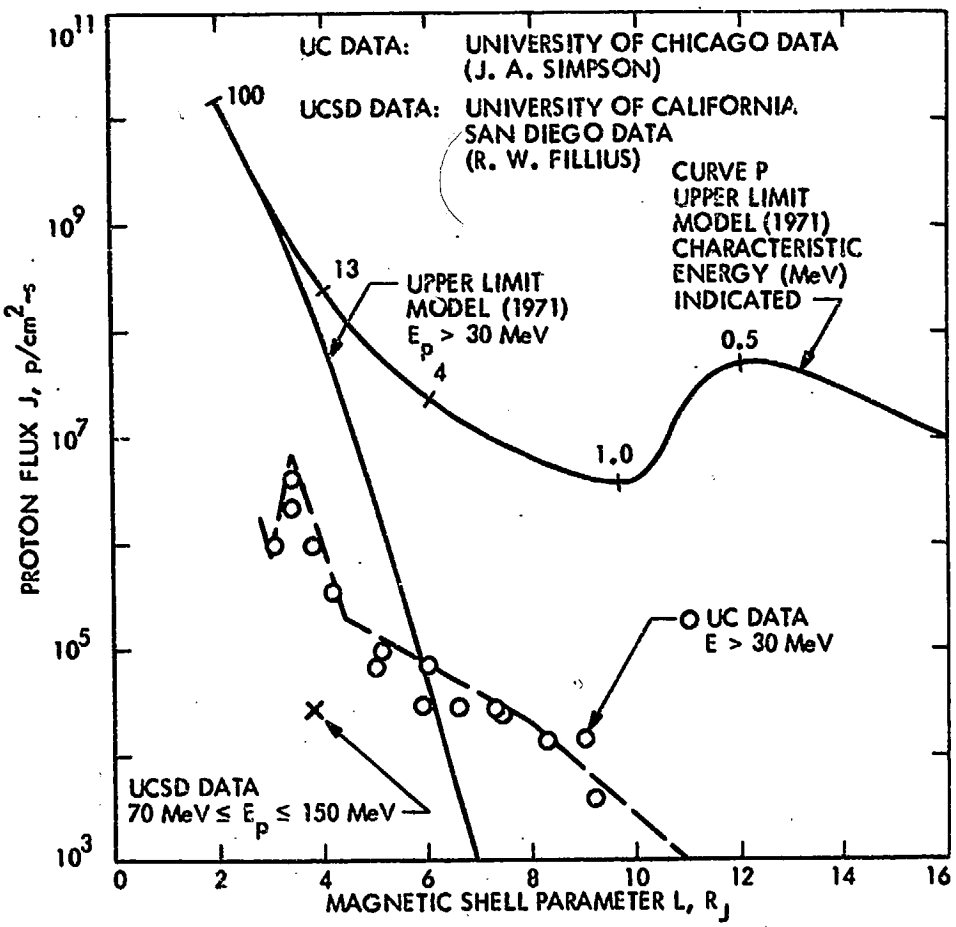

Fig. 7. Pioneer 10 experimental data and preliminary 1974 workshop data for Jupiter-trapped protons, compared with the 1971 Post-Workshop Model for protons

A typical iso-contour plot of electron flux for $E_e > 3$ MeV, based on the Pioneer workshop data, is presented in Fig. 8. The numbers at points on the Pioneer 10 trajectory shown are time in hours from perijove. The time increments between points indicate the amount of time the spacecraft spent in the high intensity field. The accumulated free-field fluence of electrons with energy greater than 3 MeV is about $7 \times 10^{12} e/cm^2$ for Pioneer 10, based on the model in Figure 8.

Figure 9 shows the particle fluxes from various Earth, Jupiter, solar, and galactic sources as a comparison. The curves represent the flux of particles with energy greater than the corresponding energy point indicated on the curves. Note that the electron fluxes in the Jupiter belts are significantly higher than Earth belt fluxes. Not only are the fluxes higher, but also the spatial distribution is so extensive for the Jovian belts that significant fluences are encountered even at 10 R_J to 12 R_J perijove flybys. However, the Jovian protons are not even as numerous or energetic as the protons from extremely large solar events at 1 AU.

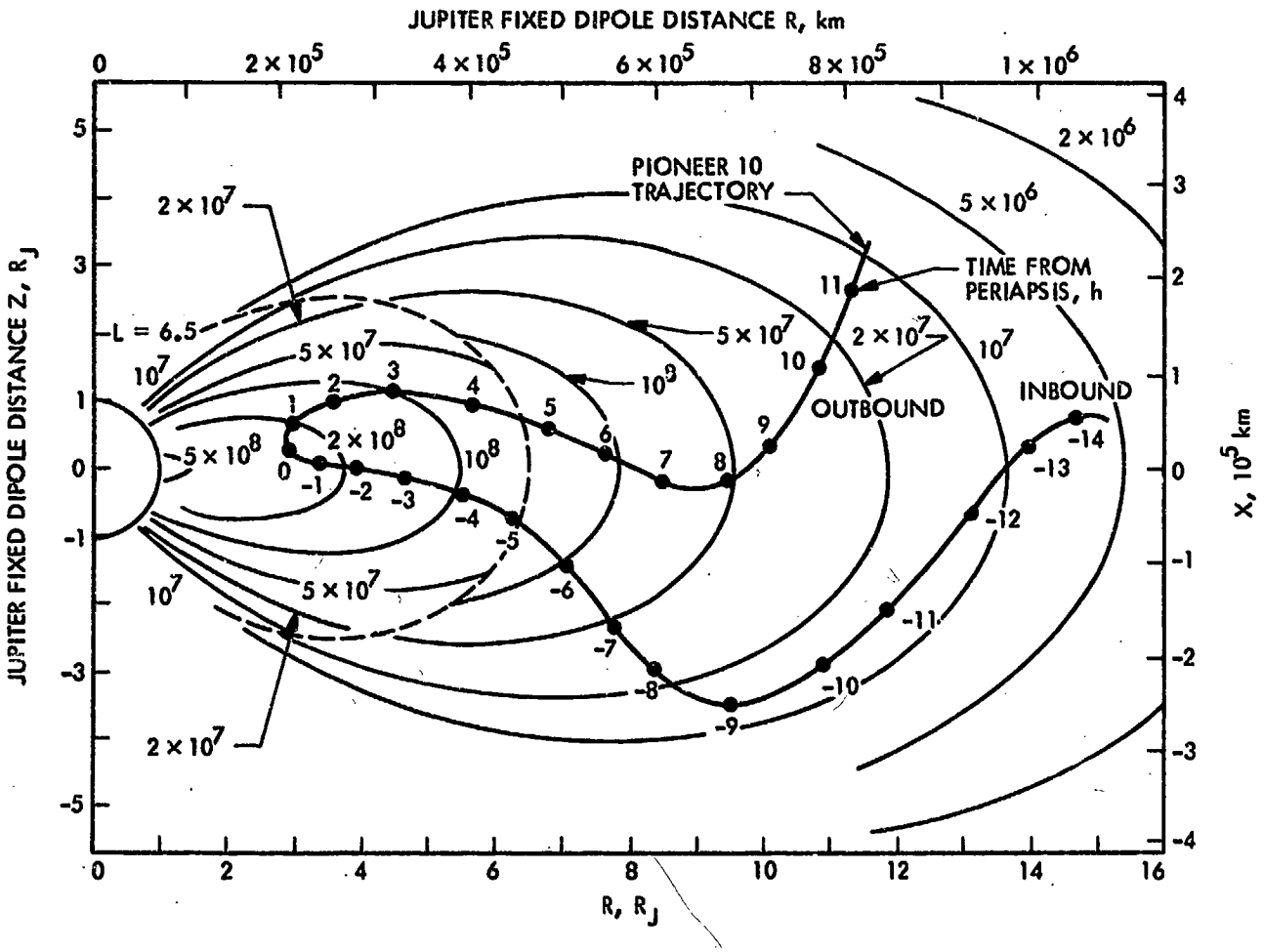

Fig. 8. Contours of constant flux J (e/cm^2 -s) of electrons $E_e > 3$ MeV based on preliminary 1974 workshop data (Joviomagnetic coordinates assuming longitudinal symmetry)

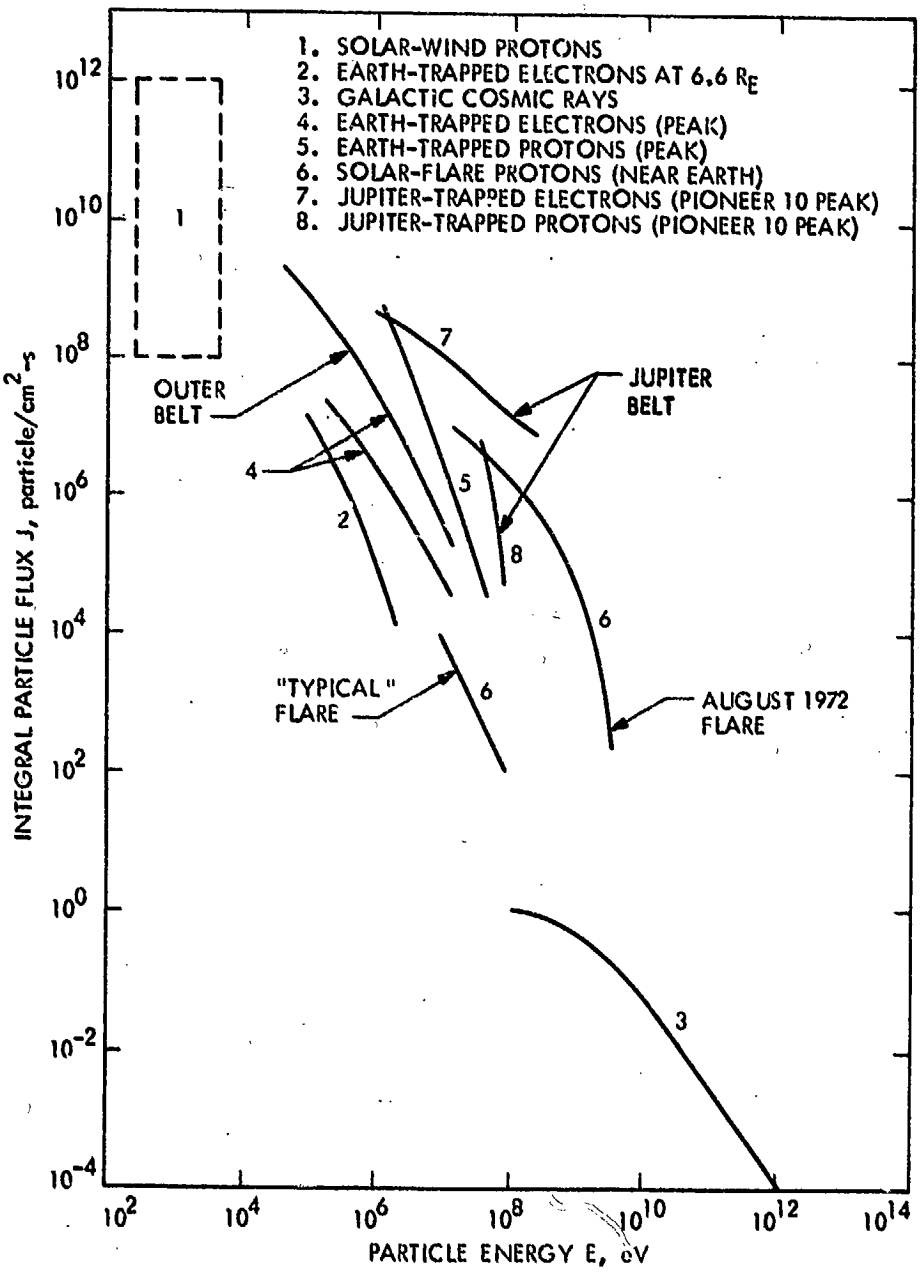

Fig. 9. Comparison of electron and proton integral fluxes for Earth, Jupiter, solar and galactic environments

For the MJS77 spacecraft design (Fig. 10), the electron and proton environments have been evaluated for selected equatorial Jupiter flyby trajectories having perijove distances of 5.0, 8.8 and 12 R_J. The corresponding $E_e > 3$-MeV electron fluences are 5×10^{12}, 3×10^{12}, and 10^{12} e/cm^2, respectively. The integral electron spectra for peak flux J ($>E_e$) and fluence F ($>E_e$), shown in Table 1 and Fig. 11, were derived by extrapolating the $E_e > 3$ MeV Pioneer workshop data to other energies. It is important to note that the electron environments due to galactic cosmic rays and solar flare events at all energies shown are negligible in comparison to the spectra in Fig. 11 for Jupiter flyby spacecraft. The near-Jupiter electron spectra are still being derived from the Pioneer 10 data.

Table 2 shows the integral peak flux and fluence of Jupiter protons for the same trajectories at energies $E_p > 30$ and $E_p > 70$ MeV, and for solar protons at $E_p > 30$ MeV. The integral energy spectra for solar protons are derived from a model of events which represent the accumulation expected during the MJS77 mission. The levels are shown at $E_p > 30$ MeV for purposes of comparison. The model solar spectrum is proportional to $E_p^{-1.55}$ and $E_p^{-1.87}$ for peak flux and fluence, respectively, where E_p is the proton energy (Ref. 22). For the trajectories being studied for the MJS77 mission, solar protons dominate those from galactic cosmic rays and from Jupiter, except where entries exist in Table 2. The near-Jupiter proton spectra are still being derived from the Pioneer 10 data. The absence of proton data at low energies requires caution in ignoring these particles for flyby spacecraft having perijoves within 5 R_J.

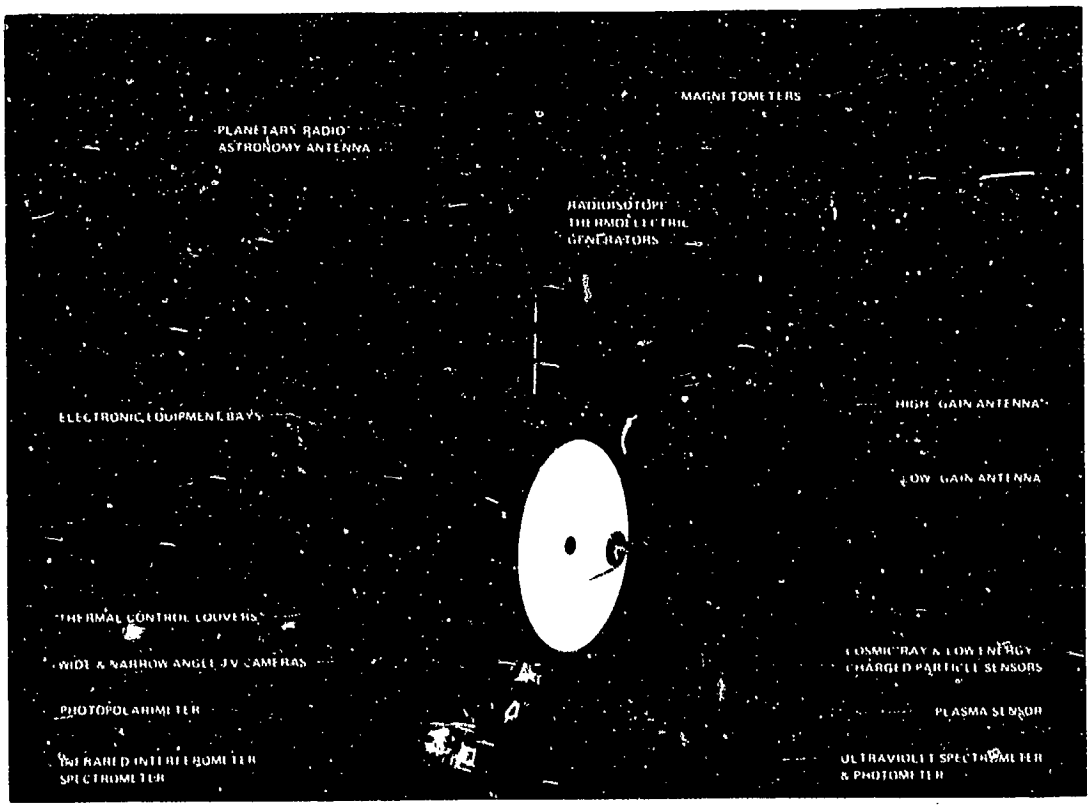

Fig. 10. The Mariner Jupiter/Saturn 1977 spacecraft

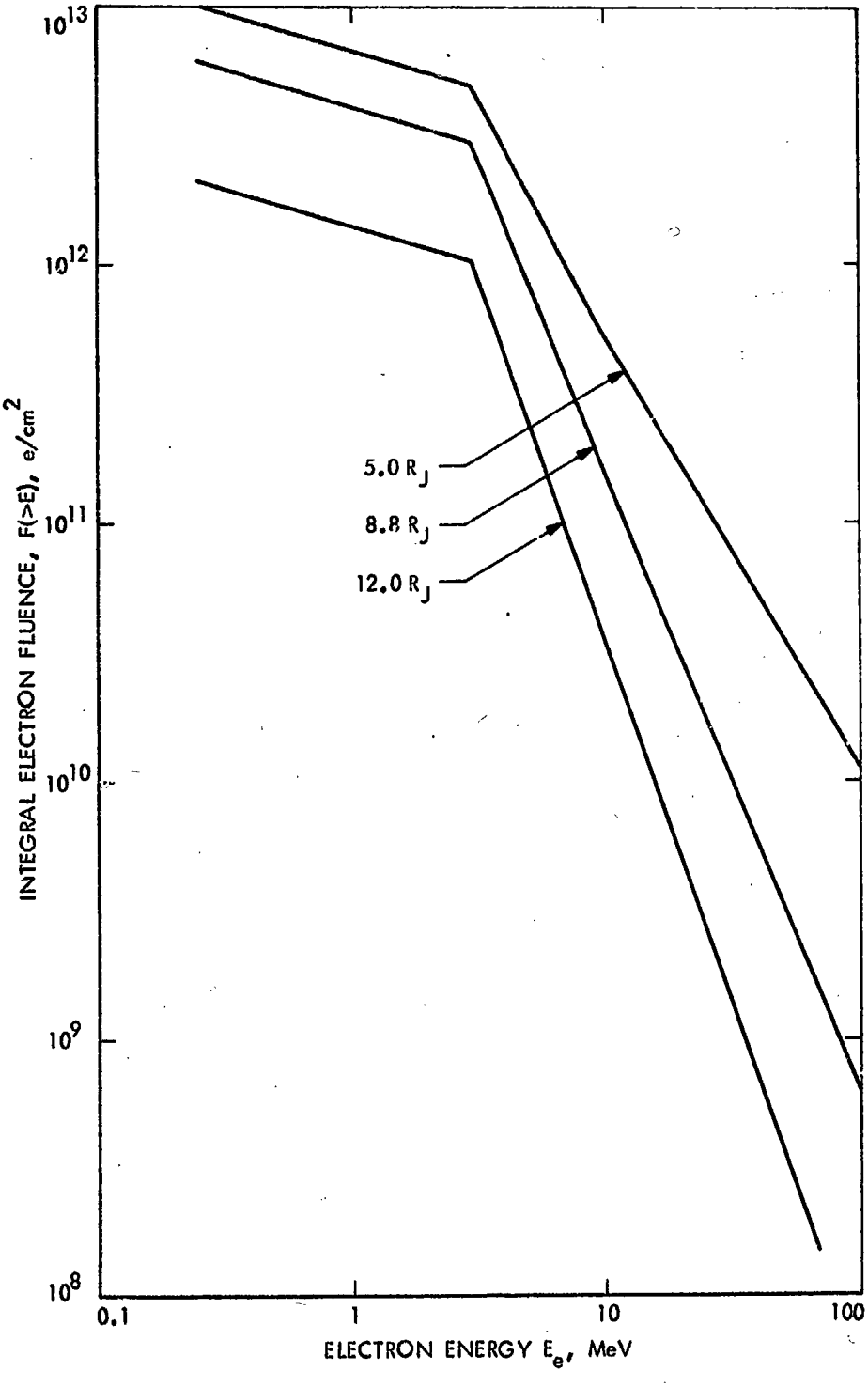

Fig. 11. Integral electron fluence energy distribution for selected perijove distances

Table 1. Free-field Jupiter electron spectra

Energy E_e MeV	Peak Flux, $J(>E_e)$, e/cm^2-s, for perijove distance, R_J			Fluence $F(>E_e)$, e/cm^2, for perijove distance, R_J		
	5.0	8.8	12.0	5.0	8.8	12.0
0.25	3.5×10^8	1.5×10^8	4.0×10^7	1.0×10^{13}	6.1×10^{12}	2.1×10^{12}
0.40	3.0×10^8	1.3×10^8	3.4×10^7	9.0×10^{12}	5.3×10^{12}	1.8×10^{12}
0.64	2.6×10^8	1.1×10^8	3.0×10^7	7.8×10^{12}	4.6×10^{12}	1.6×10^{12}
1.0	2.3×10^8	9.6×10^7	2.6×10^7	6.8×10^{12}	4.0×10^{12}	1.4×10^{12}
3.0	1.6×10^8	6.9×10^7	1.9×10^7	4.9×10^{12}	2.9×10^{12}	1.0×10^{12}
5.0	6.0×10^7	2.2×10^7	4.9×10^6	1.8×10^{12}	8.3×10^{11}	2.3×10^{11}
10	1.5×10^7	4.6×10^6	7.8×10^5	5.2×10^{11}	1.6×10^{11}	3.3×10^{10}
21	3.5×10^6	8.7×10^5	1.1×10^5	1.4×10^{11}	2.6×10^{10}	4.2×10^9
31	1.6×10^6	3.6×10^5	4.0×10^4	7.6×10^{10}	1.1×10^{10}	1.4×10^9
40	9.7×10^5	2.0×10^5	2.0×10^4	5.0×10^{10}	5.8×10^9	7.1×10^8
65	3.7×10^5	6.9×10^4	5.6×10^3	2.3×10^{10}	1.8×10^9	1.0×10^8
100	1.6×10^5	2.6×10^4	1.8×10^3	1.2×10^{10}	6.7×10^7	5.7×10^7

Table 2. Free-field proton environments

Environment	Peak Flux $J(>E_p)$, $p/cm^2\text{-}s$	Fluence $F(>E_p)$, p/cm^2
Solar particle events[a], E_p >30 MeV	1.3×10^4	2.0×10^9
Jupiter protons, E_p >30 MeV 5.0 R_J	1.5×10^5	1.0×10^9
8.8 R_J	9.0×10^3	$<10^7$
12.0 R_J	$<10^3$	$<10^6$

[a] The probability is 95% that these levels will not be exceeded.

III. SIMULATION OF JUPITER RADIATION ENVIRONMENT

A. Simulation of Electrons and Protons

The inadequacy of analytic evaluation to determine accurately the radiation effects in material and electronic parts and to predict the resultant consequences to complex systems makes experimental simulation a practical necessity. Limitations of existing facility capabilities makes it necessary to simulate effects rather than to reproduce the expected radiation environment in these facilities. In order to determine the test requirements appropriately, several parameters must be understood. For example, the test may require rate acceleration from the actual expected rate. The spectrum may require simulation and isotropic exposures may not be practical.

At test energies above ~10 MeV, a cyclotron or LINAC may be used. The LINAC or cyclotron may be used where rate interference is known to be negligible or where just total damage effects are being simulated. The LINAC has been used to irradiate complementary metal oxide on silicon (CMOS) devices because they are considered to be insensitive to radiation rate, at least at average fluxes of $\leq 10^{10}$ e/cm^2-s. However, at average fluxes $\geq 10^{11}$ e/cm^2-s, electric fields build up across dielectrics in CMOS and may cause electrical breakdown effects.

As mentioned, the environment to be simulated has a spectral distribution. Monoenergetic tests are conveniently utilized to reproduce the damage and interference of the expected spectrum. The test energy is determined by collapsing the energy spectrum using appropriate equivalences of the spectrum to the test energies.

If the nature of the damage mechanism can be determined a priori, then it may become possible to simulate realistically the space environment with other types of radiation, for example fission neutrons or Co^{60} gammas. These are considerably more convenient to use in radiation effects simulation. Since the damage to CMOS is predominantly due to ionization, the total dose damage concept makes particle subsitution, for example, Co^{60} gammas for electrons, quite appropriate. However, previous data have shown (Ref. 23) that for CMOS devices, Co^{60} and electrons are not 1-to-1 equivalent on a specific rad basis; instead, the electrons may be more damaging by factors approaching 2. The physical differences in ionization energy deposition between gammas and electrons, plus the additional electron displacement damage, could account for this factor at least at high dosage levels $>10^6$ rad(Si) where serious effects are expected for many parts.

B. Electron and Proton Equivalencing

Relative and absolute damage functions which depend only upon the particle type and its energy have led to effective spectral simulation with single proton and electron energies. Figure 12 shows both absolute ionization dose and relative displacement damage in silicon as a function of particle energy. The data for the displacement curves are based on test results from silicon semiconductor materials and transistors; the important feature for the displacement curves is that the relative distribution is reasonably well behaved within the uncertainty indicated for p and n type materials and the energy band of interest, ~0.3 to 30 MeV. The practical advantage of energy equivalencing of displacement damage is that each type of exposure is reduced to a monoenergetic particle fluence. The practical disadvantage is that the requirement for testing in each radiation environment must be met considering

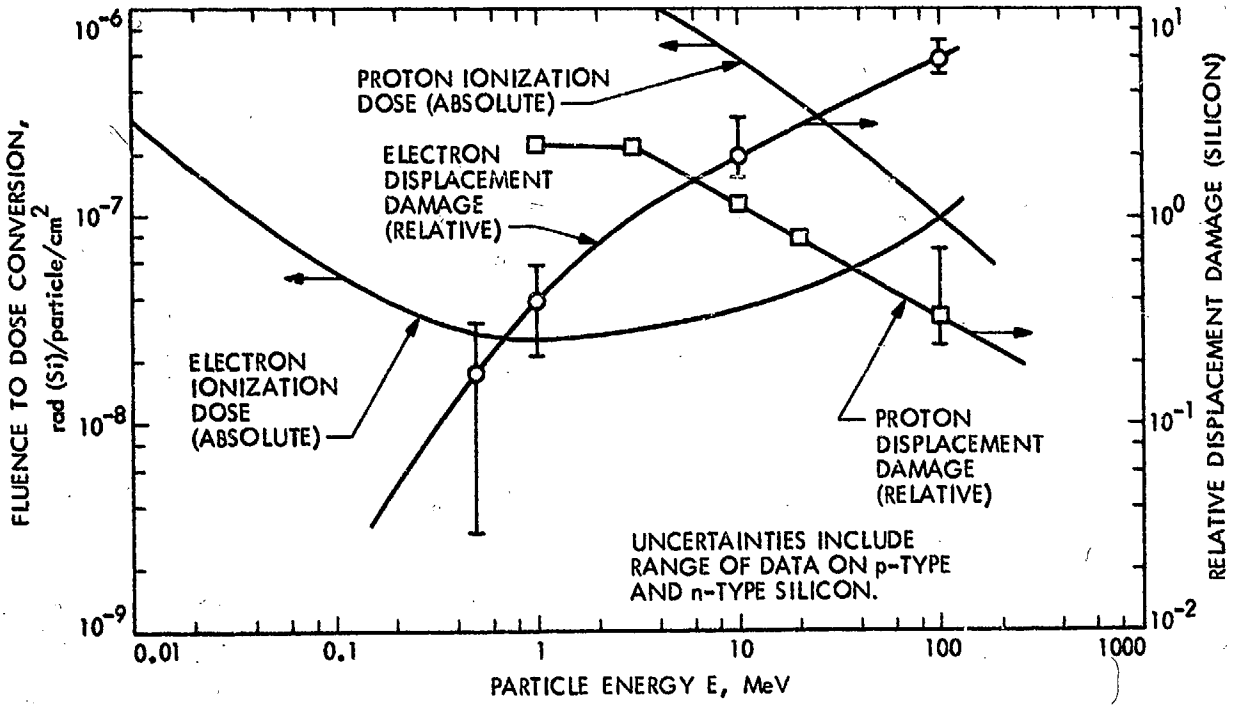

Fig. 12. Electron and proton ionization energy deposition and relative displacement damage in silicon

that different particle types vary 2 to 3 orders of magnitude in displacement damage equivalent fluences. As previously stated, the ionization dosage is generally believed to produce about the same amount of damage independent of particle energy and roughly independent of particle type within a factor of 2 to 3.

Because of the dominance of the electron environment the remainder of the discussion on test simulation is limited to electrons; but the general approach and considerations apply to protons also. Typical electron environmental estimates appropriately converted to single energy equivalent fluences and dosages integrated throughout the trajectory versus the flyby perijove distance are presented in Fig. 13. The curves in Fig. 13 specifically relate the electron fluence both as a 3-MeV equivalent of the total electron spectrum and as a total fluence having energy greater than 3 MeV. In addition, the 3-MeV equivalent fluence is specified as an ionization and displacement damage equivalent in silicon. Figure 13 also shows an electron total dose curve as a function of perijove distance. From these results, proper selection of 3-MeV test levels can be made to accommodate both ionization and displacement damage effects in candidate piece-parts, components, and circuits.

C. Accelerated Testing

Accelerated testing by exposure to higher fluxes may be necessary to employ available facilities and to perform reasonably short duration tests. A concern with accelerated testing is that the faster rates may not produce representative effects from expected mission-rates and particularly that they may be more or, even worse, less severe depending on the degradation mechanism. An example of the more severe effect is a second particle in the same region affected by the initial particle interacting with the atoms within a time shorter than the relaxation time for rapid annealing of the effect produced by the initial particle.

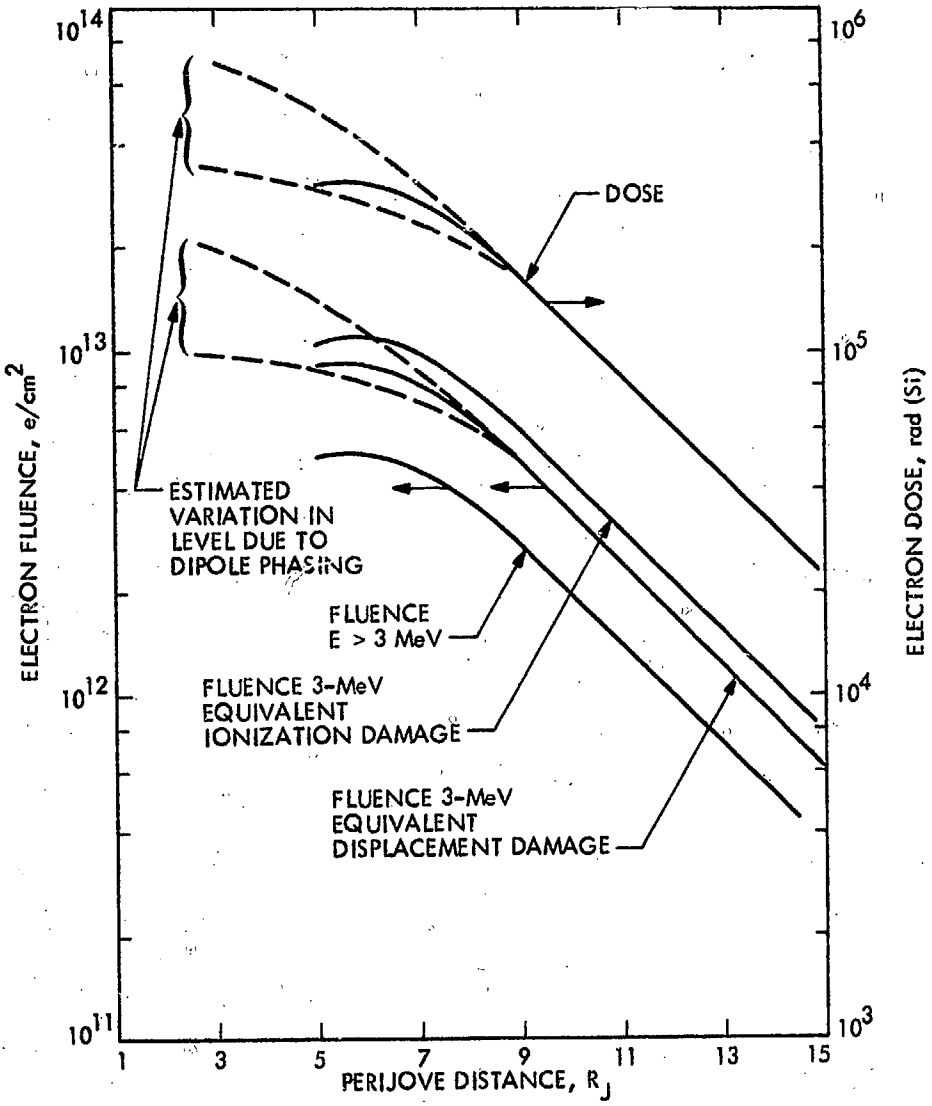

Fig. 13. Electron fluence and dose accumulation in a point detector for freefield environment and for selected trajectories versus perijove distance

Several tests were performed to consider this problem. As an example, a set of CMOS NAND gates (CD4011), were irradiated by a Co^{60} source at the rate of 220 rad(Si)/min. A second set of these gates was irradiated at 7,000 rad (Si)/min. The highest ionization considered for MJS77 corresponds to ~580 rad(Si)/min for 5×10^8 e/cm2-s(3 MeV); and, for about half the fluence, the rate is below 220 rad(Si)/min. The test indicated that within the limited statistical validity of our small sample sizes (8 to 12), the higher rates are ~30% more damaging to the most sensitive parameter, V_{TN} (N-channel threshold voltage) for one manufacturer and that there was no difference on other parameters, see Fig. 14. Results for parts from another manufacturer showed no consistent pattern. Thus the results for the gates show enhancement of the damage due to acceleration.

One type of science sensor which was tested at various electron rates was a set of channel multiplier devices. Two sources of electrons were used. One was a $Sr^{90}/Y90$ beta source ($E_e \leq 2.26$ MeV) which could be positioned to

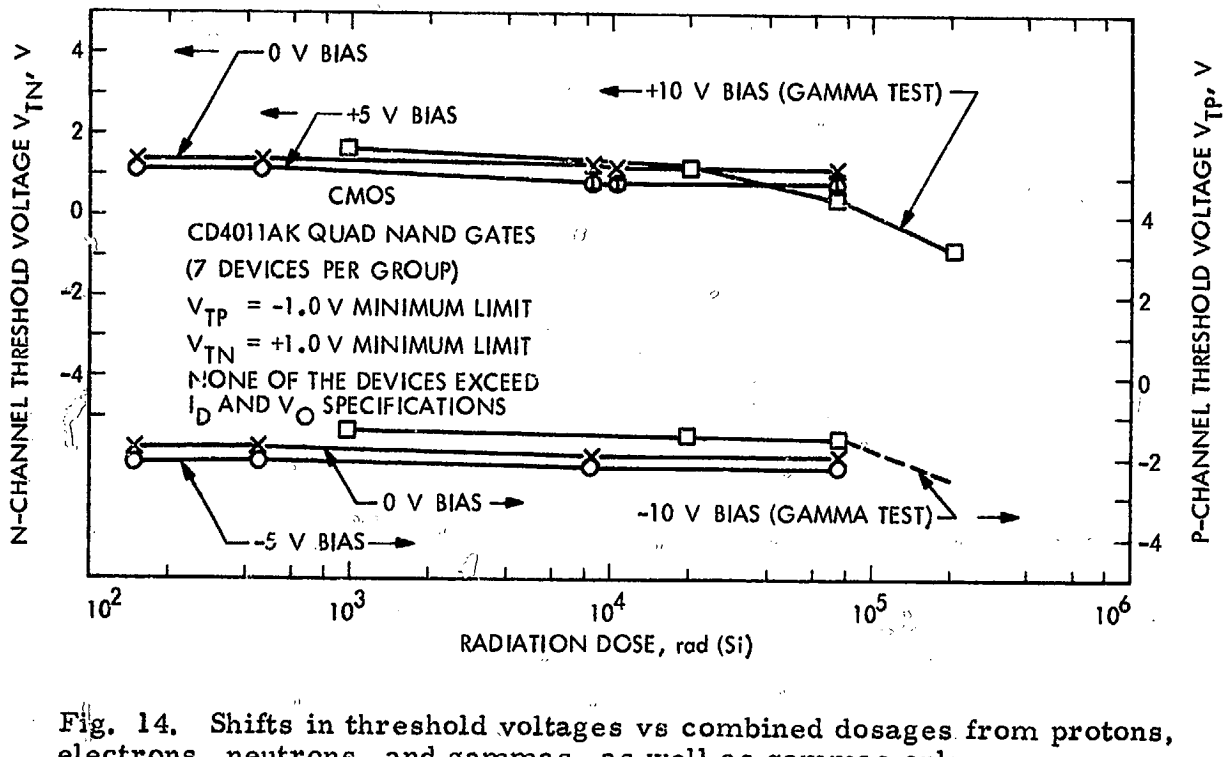

Fig. 14. Shifts in threshold voltages vs combined dosages from protons, electrons, neutrons, and gammas, as well as gammas only

produce fluxes from 4 e/cm^2-s to 2.5 × 10^3 e/cm^2-s. The second source was the JPL Dynamitron, where fluxes of 10^8 or 10^9 e/cm^2-s ($E_e \simeq 2.28$ MeV) were used to reach a final fluence of 2.23 × 10^{12} e/cm^2. For this fluence the devices degraded in signal-to-noise ratios by two orders of magnitude and were no longer useful as detectors. This problem is related to count rate effects due to high fluxes. That is, at a flux $\lesssim$10^6 e/cm^2-s, the device would be operational after fluences of 10^{13} to 10^{14} e/cm^2. With the voltage off during irradiation, the channel multiplier will operate after 10^{16} to 10^{17} e/cm^2 (3 MeV) exposures.

Another type of science device was irradiated as part of the analysis of silicon-vidicon tubes and silicon targets from similar tubes. The devices were irradiated by electrons of 1 MeV (Si targets only) and 12.5 MeV, with photons of 85 keV and Co^{60} gammas (1.17 and 1.33 MeV), and with protons of 3 MeV (Si targets only), 28 MeV, and 144 MeV (Refs. 24 and 25). The sensitive element in the Si vidicon tube is just the silicon target, which is a wafer of diodes with 5 × 10^4 diodes/cm^2. As expected, for the same absorbed dose, no difference is seen between different photon energies. However, Brucker (Ref. 24) showed that a factor of ~7 exists between 1-MeV electrons and 11-MeV electrons after normalizing by the dE/dx ratios. An explanation of this may be in the displacement damage difference ratio. If we ratio the empirical equation for displacement damage (Ref. 26),

$$D(E_e) = 0.4\left(1 - e^{-E_e}\right) E_e^{0.486}$$

for E_e = 11 MeV and E_e = 1 MeV, we find a factor of ~5, which very nearly removes the discrepancy. However caution should be used in this assessment because the sample sizes were only 3 Si targets and 3 vidicon tubes.

For energy equivalencing of protons, large variations in effects exist between 3 MeV, 38 MeV, and 140 MeV. Using the proton displacement damage curve in Fig. 12, together with the dE/dx ratios, makes the equivalent fluence at 3 MeV and 140 MeV consistent in the amount of dark current increase as seen in Fig. 15 (from over two orders of magnitude separation) and brings the 38-MeV dark currents within a factor of ~4 of the other two energies. Using the dE/dx loss in the glass envelope for the 38-MeV and 140-MeV cases does not remove all of the difference which may be due to process variations, dosimetry uncertainties, or a combination of these. The dark currents are taken at room temperature (i.e., the usual spacecraft electronic temperatures); however, dark currents can be reduced to ~0.5 nA when the Si targets are cooled to 85°K (Ref. 24).

The dE/dx value is related primarily to the ionization damage. Thus the displacement equation taken with the energy loss equation may be used to separate out the two types of damage.

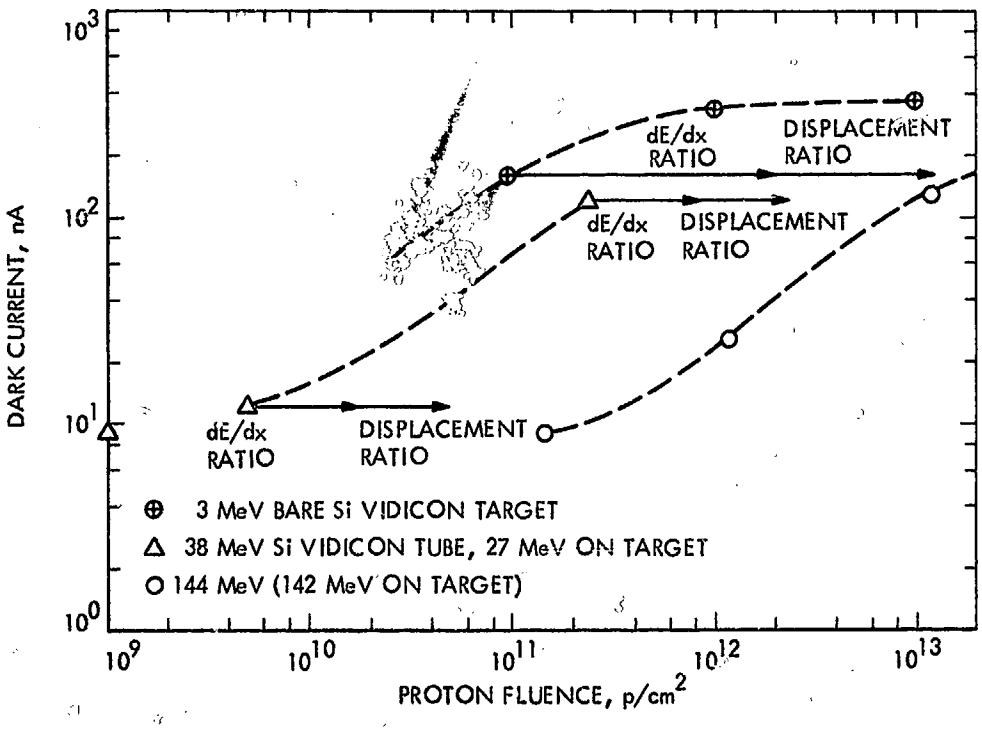

Fig. 15. Silicon vidicon dark current vs proton fluence

IV. PROTON DATA

A. Sensitive Electronics

As discussed in Section III, CMOS electrical characteristics are degraded by ionization effects. Protons produce significantly more ionization per particle than electrons and, more importantly, the relative number of displacements is several thousand times that of electrons (Ref. 18).

Because ionization degradation can be effectively evaluated by assuming that the dose-damage concept applies, the influence of particle type and energy which produces the ionization essentially can be neglected. This concept, although simplistic in nature, because it neglects deposition rates and damage concentrations, has application in the assessment of the electronic devices, which are much more sensitive to ionization damage than to displacement damage. If the proton energy is low enough, it predominantly ionizes instead of displacing the atoms in the devices. For Jovian proton fluences, both damage mechanisms prevail; however, protons in significant amounts at perijove distances >5 R_J have energies less than about 35 MeV to 50 MeV. Device cans provide shields which further reduce these energies to where the ionization due to low energy protons would prevail.

For the sensitive electronics considered, CMOS and linear operational amplifiers, ionization degradation begins at dosage levels between ~10^4 to 10^6 rad(Si) and displacement degradation at 20 MeV proton fluence levels between 10^9 to 10^{11} p/cm^2. For comparison purposes, the ionization dosage levels correspond to 20-MeV proton fluences of 3×10^{10} to 3×10^{12} p/cm^2, which implies that proton displacement degradation would also be important at these levels. Typically, this large a fluence of protons can produce significant displacement degradation in displacement-sensitive electronics. However, the Jupiter proton free-field fluence for a very close perijove (2.8 R_J) is only about 4×10^{10} p/cm^2, 20 MeV equivalent of the unshielded free-field spectrum. This was the equivalent fluence estimated from the Pioneer 10 encounter at Jupiter using data taken from Ref. 21. For MJS77, the accumulated fluence is expected to be less than 1×10^9 p/cm^2 for a 5.0 R_J perijove flyby mission. As a result, the proton environment is not expected to produce significant degradation to the sensitive spacecraft electronics. It is important to note that these levels are exposure levels which essentially are conservative estimates for devices inside the spacecraft. The conservatism applies to a lesser extent even for devices in their packages outside the spacecraft. Neglecting the spacecraft geometric shielding reduction factor and using the equivalencing approximation accounts for the conservatism, since the low energy particles, which cannot penetrate even 0.05 g/cm^2, are included in the equivalencing.

Data from recent proton radiation tests on both operational amplifiers and CMOS, which are presented in Table 3 and Fig. 14, typically show that these radiation-sensitive electronics can tolerate ~30 MeV proton fluences up to several times 10^{10} without significant degradation. This has been generally demonstrated by spacecraft in flight, i.e., by Earth-orbiting satellites and other interplanetary spacecraft operating successfully in Earth-trapped and solar protons. These tests also included combined effects of electrons and neutrons and gammas performed sequentially, but the effects of these other radiation types were negligible at the levels of this test.

The 17 flight-quality LM108A operational amplifiers showed some significant degradation in V_{OS} and I_{OS} (offset voltage and current) at

Table 3. Radiation effects on operational amplifier, LM108A (flight quality).
(Sample size - 7, $\overline{X}$ indicates mean value of sample test results)

Test condition	Spec limit	Units	Pre-irradiation measurement		Post-irradiation measurements							
					Proton, 2×10^9 p/cm^2		Electron, 3×10^{11} e/cm^2		Neutron, 2×10^{11} n/cm^2		Proton, 2.6×10^{11} p/cm^2	
			$\overline{X}$	N[a]	$\overline{X}$	N	$\overline{X}$	N	$\overline{X}$	N	$\overline{X}$	N
					I_{OS}, Offset current							
+15V bias	0.2	nA	0.003	0	0.02	0	0.04	0	0.08	0	0.19	3
Unbiased	0.2	nA	0.06[b]	0	0.08	1	0.21	1	0.29	2	1.12	4
					I_B, Input bias current							
+15V bias	2.0	nA	1.12	0	1.29	3	1.35	0	1.46	0	3.37	7
Unbiased	2.0	nA	1.28	1	1.13	1	1.41	1	1.69	1	3.95	7
			Current gain: All devices remained within the specification limit.									
+15V bias	99 min	dB	114	0	114	0	112	0	109	1	102	2
Unbiased	99 min	dB	116	0	119	0	110	0	107	0	95	7
			V_{OS}, Offset voltage									
The biased group of devices and four unbiased devices exceeded the 0.5-V limit after final proton exposure.												

[a]Number of devices exceeding the specification limit.

[b]One device excluded from the calculation due to an apparent measurement error.

2.6×10^{11} p/cm^2 (30 MeV) and with some parts showing the input bias current I_B out of specification at 2×10^9 p/cm^2. Table 3 displays the characteristic changes in these parameters under the test conditions and identifies the parameters which degraded out of specification.

The 30 each CMOS quad 2 Input NAND gates (CD4011AK) and Dual J-K flip-flops (CD4027AK) were within specification for parameters I_{DD}, V_{OL}, and V_{OH} (drain current, output voltage-low, output voltage-high) at 500 rad (Si) (2×10^9 p/cm^2). At 50,000 rad (Si) (2.5×10^{11} p/cm^2) the quad NAND gates showed acceptable stability although specification limits of 1-volt minimum was exceeded. Figure 14 shows practically no P and N Channel threshold voltage shifts under proton irradiation to 10^5 rad(Si). Although in this test, 10^5 rad (Si) was not exceeded, typically the degradation becomes significant as demonstrated by earlier data from Danchenko (Ref. 27). The voltages are the most sensitive parameters to radiation degradation for most applications.

B. Science Parts

Figure 15 shows one example of proton degradation in Si vidicon tubes. These devices will operate up to a dark current of 7-8 nA without degradation since the signal current can be as high as 500 nA. At higher dark currents, the contrast of the picture begins to degrade. By 100 to 200 nA of dark current, the device is essentially useless for imaging. As indicated in Section III, by cooling the vidicon target, the dark current can be reduced and the vidicon made useful again even after severe radiation damage. Fortunately, this device also is usually shielded by the lens, barrel, and camera head material. The sensor which is expected to be on MJS77 is a Se-S vidicon which has shown no permanent damage after 10^{13} p/cm^2 (140 MeV) plus 2×10^{11} p/cm^2 (38 MeV).

Protons with energies below 15 to 20 MeV can usually be shielded out of most instruments since their respective ranges are 0.34 g/cm^2 and 0.56 g/cm^2 or 50 and 82 mils of aluminum.

Prior to the Pioneer 10 encounter, protons were considered the primary environmental concern and several proton tests were performed. Reference 24 describes the type of proton test results obtained on science sensors and materials. Table 4 shows a summary of these results.

Table 4. Summary of proton irradiations of sensors and materials[a]

Component	Proton energy, MeV	Fluence, p/cm^2[b] (±20%)	Comments[b]
A/DC BB No. 1	129.5	1(10) to 7.8(12)	4 fluence points, degradation at each, powered
A/DC BB No. 2	139	2(10) to 9.5(12)	6 fluence points, degradation seen at each point
Amorphous memory and threshold switches	33	2.2(11) to 7.0(2±1)(13)	T6259 and X1147 NOL (ECD devices), no effects
Analog Multiplex "A"	144	1(10) to 1.0(13)	Degradation at each of 4 fluences, powered
Analog Multiplex "B"	135	2(10) to 8.6(12)	Degradation at each of 6 fluences
As_2S_3 lens	144	1.1(13)	<5% transmission loss
Au mirror	38	9.0(10) to 3.7(11)	No effect
BG-23 glass	144	1.3(13)	SBRC, no damage in IR region
Calcite ($CaCO_3$)	142	1.1(13)	SBRC, no damage in IR region
Calcite ($CaCO_3$)	122.5	7.0(12)	SBRC, no damage in IR region
Channel multiplier	144	1.3(13)	EMR-648-1-1 No effect
Channel multiplier	142	8.0(12)	EMR-648F, no damage
Channel multiplier	33	1.1(8)	ITT SBRC no effect
Electron multiplier	144	1.3(13)	EMR-51W, degraded gain
Epoxy	111	3.7(12)	EMR, no effect
Epoxy	100	4.0(12)	SBRC, no effect
Fused silica	144	1.2(13)	No effect in IR region, Suprasil
Fused silica	144	1.2(13)	No effect in IR region, Corning 7940
Ge (IR filter)	38	3.7(11)	SBRC, no effect in IR
HgCdTe detectors (2)	142	1.2(13)	No effect
HgCdTe detectors (2)	144	7.6(12)	No effect, LN_2 temperature in vacuum
IC (6)	38	1.8(11)	RCA COS/MOS CD 4007AD, 0.5 V shift of threshold
IR filters (9)	38	2.0(10) to 3.7(11)	SBRC, different materials, no effect
LiF	138	9.1(12)	EMR, 1216 Å (68% → 48% transmission); 1470 Å (88% → 63%)
LiF (6)	38	4.0(10) to 2.9(11)	UVLα, transmission loss
Magnetometer cell A	144	2.7(13)	Helium-filled Pyrex tube ~5% transmission (1.08μ) loss
Magnetometer cell B	142	1.3(13)	Helium filled pyrex tube ~5% transmission (1.08μ) loss
Magnetometer filter	142	1.4(13)	No effect
Magnetometer polarizer A	144	2.7(13)	~5% transmission loss (1.08μ)

a) All devices were tested passively (i.e., nonpowered electrically), at room temperature and in air unless otherwise noted.

b) Numerical notation example: 3.7(11) = 3.7×10^{11}.

Table 4. Summary of proton irradiations of sensors and materials (contd)[a]

Component	Proton energy, MeV	Fluence, p/cm^2[b] (±20%)	Comments[b]
Magnetometer polarizer B	142	1.3(13)	~5% transmission loss (1.08)
Magnetometer sensor unit	38	6.4(10) to 4.6(11)	Active test, no interference or damage in least sensitive mode, PbS
MgF crystal	144	1.2(13)	SBRC, no effect in IR
MgF crystal	138	9.1(12)	EMR, 1216 Å (52% → 50% transmission): 1470 Å (80% → 82%)
M_gF (5)	38	6.0(10) to 2.9(11)	UVLσ, no effect
PbS detector	33	2.4(11)	Actively monitored, no interference or damage ($\phi_p \approx 10^8$ p/cm^2 - s)
PbS detectors (2)	138	9.1(12)	No effect for λ = 1.08μ detection
PbS detector	142	9.8(12)	Opt. No: 20, no effect at λ = 1.08μ
Photomultiplier	144	1.3(13)	EMR 531E-01-14: loss of Q. E. and radiant sensitivity
Photomultiplier	144	1.3(13)	EMR 541E-02-14: gain unstable
Photomultiplier	144	1.3(13)	EMR 542G-08-18: loss of Q. E. in UV, gain OK
Photomultiplier	144	1.3(13)	EMR 543N-01-14: gain down X15 - X50: loss of Q.E. and radiant sensitivity
Photomultiplier (2)	142	8.0(12) and 1.0(13)	RCA-C70114F, bias 1.7 kV: 17% and 46% gain loss, 1% and 3% resolution loss
Photomultiplier	142	1.1(13)	RCA-C70114F, 47% gain and 2% resolution losses
Photomultiplier	142	8.9(12)	RCA-C70114M, bias 1.7 kV: 67% gain and 2.5% resolution losses
Photomultiplier	142	8.3(12)	RCA-C70114M, 56% gain and 1.5% resolution losses
Photomultiplier (2)	38	4.0(10) and 2.5(11)	ITT-F4085, no effect
Photomultiplier (2)	33	9.3(6); 9.6 and 10.7(7); 15(9)	RCA-C31034 Active test, dark current up to 2 to 4 orders of magnitude
Photomultiplier	33	0.9(7); 1.09(8)	RCA C31034 Dark current up 2 to 4 orders of magnitude, no damage at max current ratings.
Schott filter glasses (6)	122.5	7.0(12)	SBRC IR different types, no effect
Si detector (2)	144 and 142	1.1(13) and 1.4(13)	Intrinsic IR (1.08μ), S/N decrease by an order of magnitude
Si detector	33	1.0(8)	Unpowered, SBRC
Si detector	33	2.4(11)	Intrinsic IR (1.08μ), actively monitored, ϕ_p 0.9 to 1.2(8) p/cm^{2}s, total interference and significant permanent damage
	33	9.3(7) [2±1]	Active +30 mV offset 15 to 60 mV noise; no permanent damage

a) All devices were tested passively (i.e., nonpowered electrically), at room temperature and in air unless otherwise noted.

b) Numerical notation example: 3.7(11) - 3.7×10^{11}.

Table 4. Summary of proton irradiations of sensors and materials (contd)[a]

Component	Proton energy, MeV	Fluence, p/cm^2[b] (±20%)	Comments[b]
Si IR filter	144	1.2(13)	SBRC, no effect
Si IR filter	38	3.7(11)	SBRC, no effect
Silicon resin block	144	1.2(13)	SBRC, no effect in IR
Silicon resin between two fused silica pieces	144	1.2(13)	SBRC, no effect in IR
Silicon resin between yellowed fused silica	144	1.2(13)	SBRC, no effect in IR
Thermopile	144	1.3(13)	SBRC, no effect in IR (M69-16)
Thermopile	38	3.9(11)	SBRC, no effect
Vidicon, Se-S (2)	144	6.8(10)	G.E. 1341-02, no effect
Vidicon Se-S	144	1.3(13)	G.E. 1341-02, slight effect
Vidicon, Se-S (3)	38	2(9), 2(10) and 2.3(11)	G.E. 1341-02, after 144 MeV exposures, no effect
Vidicon, Si(2)	144	6.8(10)	RCA 4532, significant damage
Vidicon Si	144	1.3(13)	RCA 4532, seriously damaged
Vidicon Si targets(9)	142	1.1(11), 8.3(11) and 1.2(13)	RCA, 3 at each fluence level, effect not seen at lowest level (limited by technique), serious damage at other two levels
Vidicon, Si (3)	38	1(9), 5(9) and 2.4(10)	RCA 4532, seriously damaged at two higher levels, damage at lowest level
Vidicon, SIT	144	6.8(10), 1.3(13)	RCA 4804; no effect for unenhanced picture at low fluence, seriously damaged at high fluence
Vidicon, SIT	38	3(10)	RCA 4804; significant and serious damage respectively
Visible region filters (6)	38	1.3(11), 3.9(11)	Various band pass filters; no data

a) All devices were tested passively (i.e., nonpowered electrically), at room temperature and in air unless otherwise noted.

b) Numerical notation example: 3.7(11) - 3.7×10^{11}.

A. Sensitive Electronics

Although CMOS in general are quite "hard" to displacement radiation effects, their sensitivity to ionization effects due to charge storage in the insulating gate dielectric is cause for concern to the spacecraft designer. Briefly, ionizing electrons interact with the atoms of the oxide, producing hole-electron pairs in the volume of the oxide material. The electrons, having a higher mobility than the holes, preferentially diffuse away, leaving the positively charged holes to be trapped. This positive charge trapping is greatly influenced by the gate oxide field. The trapping is sensitively associated with energy states of impurity atoms in the oxide. The interface states trap charge most effectively near the negative electrode where the charge has its greatest effect on device operation by altering the critical threshold voltage. The result of ionizing radiation on the CMOS is to cause a negative shift of the threshold voltage (of both the P-channel and the N-channel), shifting the entire transfer curve less positive and increasing the leakage in the N-channel until it becomes impossible to turn the device off. A larger positive bias applied to the gate will cause a larger threshold shift.

Many attempts have been made by various investigators (Refs. 28-32) to "harden" the oxide by means of either diminishing the population of impurity atoms, i.e., producing a "clean oxide," or the addition of other compensating impurity atoms to produce a balance or stoichiometry in the oxide. Unfortunately for the spacecraft designer, the above devices are not available commercially in any quantity at the present time (1974). Some commercial CMOS gates which are state-of-the-art devices show very large shifts in threshold voltage (V_T) and large increases in the quiescent supply current (I_{DD}) after radiation doses of only 20,000 rad (Si) from Co^{60} (or the ionization equivalent $\sim 1.5 \times 10^{11}$ e/cm^2 at 3 MeV).

Radiation exposure testing of operational amplifiers (e.g., LM 108) has shown results as diverse as the following:

(a) 100% failure of test devices at 10^{11} e/cm^2 (3 MeV).

(b) 30% failure at 10^{11} e/cm^2.

(c) Nothing measurable happening at 10^{11} e/cm^2.

Low level failures [as low as 500 rad (Si)] have been attributed to a leaking current source in the operational amplifier. Several failure mechanisms are found, including charge build-up in the oxide and leaking. The results of radiation sensitivities are well known to be process-dependent, with some manufacturers showing lower sensitivities by factors of 5 in the fluence to cause the same damage. Thus operational amplifiers are difficult to screen, since after processing some devices may need only a little more radiation to invert the device. Operational amplifiers contain elements such as neutron-sensitive lateral PNP transistors and superbeta transistors that are known to be suspect in a radiation-environment. More recent LM 108's, compared with older devices, are better balanced and have an input offset current of two orders of magnitude less. Unfortunately, the radiation tolerance for this parameter may be two orders of magnitude less for the newer devices. The results for operational amplifiers as for CMOS indicate the trend of damage to be possibly process-dependent and that some devices show a radiation-induced change while others in the same exposure do not.

The results of various tests on CMOS with electrons at 3 and 20 MeV are shown in Tables 5 to 7. From these results it is apparent that widespread, diverse radiation-induced changes have taken place. It also appears that observed failures may be correlated to the date code (see Table 7), with the unfortunate trend being toward increased device sensitivity. Statistical evaluation of 3 and 20 MeV test data on CMOS by Barengoltz (Ref. 33) shows that within normal uncertainty there is no significant energy-dependence in the electron-irradiated CMOS response.

B. Science Parts

Many of the electron test results available are new and consequently the radiation effects on qualitative assessments. Table 8 lists the devices tested, the electron fluence levels and energies along with an assessment of the results.

The radiation-degradation identified in Table 8 may be reduced to acceptable levels at fluences between 1×10^{12} and 1×10^{13} e/cm^2, which are of concern to MJS77 with minimum compromise of the science objectives. However, the use of spacecraft and instrument inherent shielding is expected to provide valuable design margin.

Table 5. Conditions and gross results of electron test

Lot No.	Run No.	Type	Test conditions[a]			No. Parts	No. of failed parts[b]	
			Fluence, e/cm^2	Ave. Flux, e/cm^2-s	Energy, MeV		Marginal	Catastrophic
1	6	CD4012AD	1.4×10^{12}	1.4×10^{9}	3	10	0	0
1	6, 7, 10	CD4012AD	6.8×10^{12}	4.8×10^{9}	3	10	6	0
1	6, 7, 10, 12	CD4012AD	1.8×10^{13}	1.5×10^{10}	3	11	11	0
2	13	CD4049AD	1.3×10^{12}	1.6×10^{9}	3	8	0	0
2	13, 14	CD4049AD	5.6×10^{12}	4.8×10^{9}	3	8	8	0
2	13-17	CD4049AD	2.5×10^{13}	2.0×10^{11}	3	7	—	7
3	18	CD4014AD	1.1×10^{12}	1.5×10^{9}	3	8	0	0
3	18, 21	CD4014AD	5.6×10^{12}	5.0×10^{9}	3	9	2	0
3	18, 21-23	CD4014AD	2.3×10^{13}	1.8×10^{10}	3	9	1	3
4	19	UL02	9.5×10^{11}	1.4×10^{9}	3	11	0	0
4	19, 20	UL02	5.1×10^{12}	5.2×10^{9}	3	11	10	1
5	27	CD4011AK	1.1×10^{12}	2.0×10^{10}	3	9	5	0
5	26	CD4011AK	4.6×10^{12}	1.8×10^{10}	3	9	0	6
5	24, 25	CD4011AK	1.4×10^{13}	1.8×10^{10}	3	9	2	7
5	102	CD4011AK	5.5×10^{12}	3.7×10^{9}	3	9	0	5

Table 5. Conditions and gross results of electron test (contd)

Lot No.	Run No.	Type	Test conditions[a]			No. Parts	No. of failed parts[b]	
			Fluence, e/cm^2	Ave. Flux, e/cm^2-s	Energy, MeV		Marginal	Catastrophic
6	100, 101	CD4011AK	5.5×10^{12}	3.7×10^{9}	3	8	0	2
6	116, 117	CD4011AK	3.4×10^{12}	4.0×10^{9}	20	7	0	0

[a] V_{DD} = 10 V for irradiation and electron test. Peak flux ≅ 1000 × average flux.

[b] Failure Definition:

Type	Marginal	Catastrophic
CD4011AK	V_{IL} <3 V when V_O (unloaded) = 7 V	V_{OH} (loaded) < 5 V when V_I = 0.5 V
CD4012AD	V_{OH} (unloaded) < 7 V when V_I = 2.9 V	V_{OH} (unloaded) < 5 V when V_I = 0 V
CD4014AD	I_{OL} < 0.2 mA when V_O = 0.5 V	I_{DD} > 8 mA and I_{OL} ≤60 μA
CD4049AD	V_{OH} (unloaded) <7 V when V_I = 1.9 V	V_{OH} (unloaded) < 5 V when V_I = 0 V
UL02	V_{OL} (unloaded) > -3.5 V when V_I = -9 V	V_{OL} (unloaded) > -7.5 V when V_I = -9 V

Table 6. CD4011AK CMOS gates

Parameter	Conditions V_{DD} = 10 V	Initial value	Value after 5×10^{12} e/cm^2	
			Noncatastrophic	Catastrophic
Input current	V_I = 5	< ± 1 nA	No changes	No changes
Quiescent supply current	Inputs at V_{DD}	< 1 nA	≤ 2 nA	≤ 2 nA
	Inputs at gd. (10 min)	≤ 1 nA	39 - 62 μA	10 - 13 mA
	(24 hrs)		2.7 - 7.6 μA	8 - 9 mA
V_{OH} (loaded)	(0.6 mA 0 V bias	9.6 - 9.8 V	9.6 - 9.7 V	9.5 - 9.6 V
	(V_I = 0.5) 10 V bias	9.6 - 9.8 V	9.5 - 9.7 V	0.6 - 1.3 V
V_{OH} (unloaded)	V_I = 0.5 0 V bias	9.98 V	9.98 V	9.91 - 9.98 V
	10 V bias	9.98 V	9.96 V	0.75 - 1.4 V
V_{OL} (loaded)	(0.5 mA) 0 V bias	0.1 - 0.2 V	0.20 - 0.25 V	0.12 - 0.20 V
	(V_I = 9.5) 10 V bias	0.1 - 0.2 V	0.20 - 0.21 V	0.06 - 0.15 V
V_{OL} (unloaded)	V_I = 9.5 0 V bias	1 mV	Little change	Little change
	10 V bias	1 mV	Little change	Little change
N-channel threshold voltage, V_{TN} at 10 μA	0 V bias	1.2 - 1.9 V	1.5 - 2.0 V	-(0.4 - 1.1) V
	10 V bias	1.2 - 1.9 V	0.05 - 0.2 V	-(1.9 - 2.9) V
P-channel threshold voltage, V_{TP} at 10 μA	0 V bias	-(1.6 - 2.3) V	-(2.7 - 2.9) V	-(2.2 - 3.1) V
	10 V bias	-(1.6 - 2.3) V	-(2.3 - 2.5) V	-(2.8 - 4.1)V

Table 6. CD4011AK CMOS gates (contd)

Parameter	Conditions V_{DD} = 10 V	Initial value	Value after 5×10^{12} e/cm^2	
			Noncatastrophic	Catastrophic
V_{IL} (unloaded) V_O = 7 V	0 V bias	3.7 - 5.0 V	4.2 - 4.9 V	2.6 - 3.8 V
	10 V bias	3.7 - 5.0 V	3.4.- 3.9 V	0 V
V_{IH} (unloaded) V_O = 3 V	0 V bias	3.9 - 5.2 V	4.3 - 5.1 V	2.7 - 4.0 V
	10 V bias	3.9 - 5.1 V	3.7 - 4.2 V	0 V

Table 7. Failures vs date code

Electron tests (3 MeV)	Number of catastrophic failures/number of devices in test		
	10^{12} e/cm^2 (3×10^4 rad)	5×10^{12} e/cm^2 (1.5×10^5 rad)	2×10^{13} e/cm^2 (6×10^5 rad)
CD4011 gates (Aug. 1973)	0/9	11/18	7/9
CD4011 gates (Mar. 1973)		2/8	
CD4049 buffers (screened) (Feb. 1973)	0/8	0/8	7/7
CD4012 gates (screened) (Oct. 1972)	0/10	0/10	0/11
Gamma tests, rad (Si)	2×10^4	7×10^4	2×10^5
CD4011 gates (June 1972)	0/15	0/6	0/6

Table 8. Electron test summary for science parts

Description	Fluence, e/cm^2 (± 18%)	Electron energy, MeV	Remarks
Channel multipliers (4)	10^{10}, 2×10^{10}, 1.2×10^{11}, 2.2×10^{11}, 1.2×10^{12} and 2.2×10^{12}	2.28	Fluxes of 10^8 and 10^9 e/cm^2 (Si) gain loss × 30, resolution loss × 2
CsI substrate (2) 1 coated and in Al ring 1 uncoated and unmounted	1.9×10^{12}	1.65 to 1.70	Scintillation photographically observed at fluxes from 10^8 e/cm^2 -s to 10^{10} e/cm - s
	1.93×10^{13} 3.48×10^{12}	2.75 to 3.0 17.5 to 18.0	Transmission at 5800 Å down 3% after 3 MeV plus 2% more after 20 MeV, no loss in IR (2μ to 40μ) except at H_2O) line; no effects attributed to irradiation.
Filter lens - neon TI 535500-1 (1)	9.83×10^{11} plus 1.93×10^{13}	1.65 to 1.70 2.75 to 3.0	Transmission changed from 58% to 22% at 6929Å line.
Filter lens - neon TI 535500-1 (1)	3.48×10^{12}	17.5 to 18.0	Relative transmission changed from ~55% to ~41% at 6929 Å line.
Filters MgF_2 (3) Filters LiF (4)	9.83×10^{11} plus 2.1×10^{13}	1.65 to 1.70 2.75 to 3.0	LiF degraded ~43% at 1216Å MgF_2 degraded ~20% at 1216Å

Table 8. Electron test summary for science parts (contd)

Description	Fluence, e/cm^2 (± 18%)	Electron energy, MeV	Remarks
GaAs LED TIXL10 (1)	1.9×10^{12}	1.65 to 1.7	No change in forward voltage after either exposure (same used in both tests; small output intensity changes of 6% and an additional 3%.
	1.93×10^{13}	2.75 to 3.0	
	3.48×10^{12}	17.5 to 18.0	
Hydrogen absorption cell	0.589, 6.2, 21.1, 7.04×10^{11}	1.65 to 1.7 and 17.5 to 18.0	No data
Interference filters	5×10^{12}	2.75 to 3.0	Set of filters showed negligible to catastrophic (factor of 10^{-2}) transmission changes, data being reduced.
	3×10^{12}	17.5 to 18.0	
Lamp, Neon K3A TI530981-1	1.9×10^{13}	1.65 to 1.70	No effects in light intensity or starting voltage although envelope appeared to brown slightly.
	1.93×10^{13}	2.75 to 3.0	
Lamp, Neon K3A TI1530981-1	3.48×10^{12}	17.5 to 18.0	No effects in light intensity or starting voltage although envelope appeared to brown slightly.
Optical glass (set)	6.5×10^{11}	19.5 to 7.0	Transmission losses except in quartz
SK-10	5×10^{12}	2.75 to 3.0	at 4500Å transmission loss × 2.3
SF-8	1.1×10^{12}	2.75 to 3.0	× 1.2
BASF 52	5×10^{12}	2.75 to 3.0	× 2.6
Quartz	5×10^{12}	2.75 to 3.0	no effect

Table 8. Electron test summary for science parts (contd)

Description	Fluence, e/cm^2 (± 18%)	Electron energy, MeV	Remarks
Pioneer 10 spacecraft	1.9×10^{13}	3 equivalent	Degradation observed
Reticon (UV detector)			
RL-64-QN	5.2×10^{12}	2.75 to 3.0	Device failed to scan, irradiated passively
Si Detector ENL-626B 531280-1	1.9×10^{12}	1.65 to 1.70	Used to detect 6926Å neon line; No effects seen
	1.93×10^{13}	2.75 to 3.0	
	3.48×10^{12}	17.5 to 18.0	
Spectral filters			
MM'71 I-G	1.1×10^{12}	2.75 to 3.0	No effects
MM'71 I-B	1.1×10^{12}	2.75 to 3.0	
MM'71 P-B	1.1×10^{12}	2.75 to 3.0	

VI. PREDICTIONS OF SPECIFIC RADIATION EFFECTS

In general, there are no insurmountable technical problems owing to the Jovian radiation environment at the range of levels identified for potential MJS77 missions. This conclusion is considered to be valid for perijove flybys as close as 5 R_J.

Specific radiation effects expected during selected Jupiter flyby perijoves for the sensitive piece-parts, components and science devices, using available radiation susceptibility data have been projected. The most erratic performance in terms of predictability will probably be the operational amplifiers where large variances in susceptibility to ionizing radiation [10^3 to 10^6 rad (Si)] have been reported. Considering commercially available CMOS, minimum threshold degradation fluence starts at about 5×10^{11} e/cm^2 (~3 MeV). This is equivalent to about 15,000 rad (Si), which could be accumulated during the projected flight path at a 12-R_J perijove. Proper fabrication and process control and radiation screening of selected parts may increase this threshold to 10^5 rad (Si).

For science experiments both the environment and the instrument objectives and description must be considered in solving the radiation problems. The environment is usually the less controllable in this solution unless particularly hostile regions can be avoided as an option in the mission design. Examples where the option can be exercised are perijove distance and latitude/longitude selection. For instruments most tradeoffs will affect the experiment objectives. Based on the results thus far, the potential design solutions, along with the tradeoffs in mission selection, can ensure that, for levels between 10^{10} to 10^{11} p/cm^2 (20 MeV) and between 10^{12} to 10^{13} e/cm^2 (3 MeV), permanent damage is expected to be tolerable for piece-parts and components in the MJS77 spacecraft science instruments. However, some interference is expected in science instruments, and special design tradeoffs and component selection are necessary.

Any experiment which requires high precision measurements (e.g., $\leq$0.1%) or which requires measurements of very small signals (e.g., photon counting) is susceptible to degradation in its components. The exact quantitative description of what constitutes an acceptable environment depends on the function of the components in the instrument. If the instrument can be recalibrated after exposure (e.g., by observing a well known stellar source), then the instrument is again a useful measuring device with some different, but known, sensitivity. For example, ultraviolet experiments are susceptible to degradation in optical transmission. However, reflection optics are less susceptible and recalibration would be applicable to accommodate degradation.

Component selection is an effective way to design for a radiation environment. The imaging experiment is an example of hardening by component selection. By changing the transmission optics to fused silica, a high quality quartz, and radiation resistant glass, the photon intensity variation at the vidicon (wavelength dependent) is essentially eliminated during the Jovian encounter. Further, by the retention of the Se-S vidicon (with a quartz envelope) instead of the more sensitive Si vidicon, only filter and circuitry design for the radiation environment is required. Components in the imaging subsystem are expected to be capable of sustaining at least 10^{13} e/cm^2 (3 MeV). An example of science objective modification would be alteration of the observation periods associated with high flux regions near Jupiter for some of the spectroscopic investigations. None of the examples cited as specific solutions can be utilized without detailed study. The important point is that

radiation-tolerable designs demand system integration approaches which impact at the piece-part and component level as well as the spacecraft system and mission.

Presently, MJS77 is pursuing analysis, testing, and design approaches for solutions to the radiation environment problem. Circuit design analysis techniques are being applied to identify potential radiation effects at higher levels of equipment. Radiation damage and interference test programs are regularly producing data for parts selection and design application. The effects of alternate trajectory selections are also being examined. Pioneer 10 data is being studied in detail to ensure proper understanding of the radiation belt models and their implications in various missions. Screening and/or testing of flight parts is being considered; part suppliers are being consulted with regard to radiation-hardened parts. Finally, limited applications of shielding are being evaluated for special design problems. These mission and system design approaches will allow for identification and implementation of appropriate radiation design techniques.

REFERENCES

1. Roberts, M. S., and G. R. Huguenin, "The Radiation Belt of Jupiter," Memoires Soc. R. Sc. Liege, Cinquieme Serie, Tome VII, Fasc. Unique. Extrait 1962.

2. Carr, T. D., and S. Gulkis, "The Magnetosphere of Jupiter," Ann. Rev. Astron. Astrophys., Vol. 7, p. 577, 1969.

3. Chang, D. B., and L. Davis, Jr., "Synchrotron Radiation as the Source of Jupiter's Polarized Decimeter Radiation," Astrophys. J. Vol. 136, p. 567, 1962.

4. Berge, G. L., "An Interferometric Study of Jupiter's Decimetric Radio Emissions," Astrophys. J., Vol. 146, No. 3, p. 767, 1966.

5. Branson, N. J. B. A., "High Resolution Radio Observations of the Planet Jupiter," Roy. Astron. Soc. Mon. Not., Vol. 139, No. 2, p. 155, 1968.

6. Warwick, J. W., "Particles and Fields Near Jupiter," NASA CR-1685, October 1970.

7. Barber, D., and J. F. R. Gower, "The Spectral Index of the Radiation from Jupiter Between 178 and 610 Megacycles/Second," Planet. Space Sci., Vol. 13, p. 889, 1965.

8. Eggen, J. B., "The Trapped Radiation Zones of Jupiter," General Dynamics Fort Worth Division, Report FZM-4789, 1967.

9. Haffner, J. W., "Calculated Dose Rates in Jupiter's Van Allen Belts," AIAA J. Vol. 7, p. 2305, 1969.

10. Klopp, D., "Electron and Proton Flux Models for Jupiter's Radiation Belts," Proceedings of the Jupiter Radiation Belt Workshop, A. J. Beck, ed., Technical Memorandum 33-543, Jet Propulsion Laboratory, Pasadena, California, July 1, 1972, pp. 83-108.

11. Koepp-Baker, N. B., "A Model of Jupiter's Trapped Radiation Belts," General Electric, Missile and Space Division, Report No. 68SD263, 1968.

12. Luthey, J. L., and D. B. Beard, "The Electron Energy and Density Distribution in the Jovian Magnetosphere," Proceedings of the Jupiter Radiation Belt Workshop, A. J. Beck, ed., Technical Memorandum 33-543, Jet Propulsion Laboratory, Pasadena, California, July 1, 1972; see Ref. 15, pp. 47-81.

13. Thomas, J. R., and W. R. Doherty, "Calculation of Neutron Decay Proton Trapping in the Jovian Magnetosphere," see Ref. 15, pp. 315-345.

14. Divine, T. N., "The Planet Jupiter (1970)," NASA SP-8069, December 1971, and "Jupiter Radiation Belt Engineering Model," Proceedings of the National Symposium on Natural and Manmade Radiation in Space, E. A. Warman, ed., NASA TMX-2440, p. 556, Jan. 1972.

15. Beck, A. J., ed., Proceedings of the Jupiter Radiation Belt Workshop, Technical Memorandum 33-543, Jet Propulsion Laboratory, Pasadena, California, July 1, 1972; see in particular T. N. Divine, "Post-Workshop Models of Jupiter's Radiation Belts," pp. 527-542.

16. McDonald, R. R., W. S. Shipley, et al., Astronautics and Aeronautics, pp. 36-95, September 1970.

17. TOPS Project, "Thermoelectric Outer Planets Spacecraft (TOPS) Advanced Systems Technology Project, Final Report," JPL TM-33-589, April, 1973.

18. Larin, F., Radiation Effects in Semiconductor Devices, John Wiley & Sons, pp. 211-212, 1968.

19. Shawhan, S. D., D. A. Gurnett, R. F. Hubbard and G. Joyce, "Io-Accelerated Electrons: Predictions for Pioneer 10 and 11," Science, Vol. 182, p. 1348, Dec. 28, 1973.

20. Mead, G. D., and W. N. Hess, "Jupiter's Radiation Belts and the Sweeping Effect of Its Satellites," JGR, Vol. 78, No. 16, pp. 2793-2811, June 1, 1973; also W. N. Hess, "More About Jupiter's Radiation Belt," NOAA TM ERL OD-19, Nov. 1973.

21. Science, Vol. 183, No. 4122, Jan. 25, 1974: see, for example, E. J. Smith, et al., "Magnetic Field of Jupiter and Its Interaction with the Solar Wind," p. 305; J. A. Simpson, et al., "Protons and Electrons in Jupiter's Magnetic Field: Results from the University of Chicago Experiment on Pioneer 10," p. 306; J. A. Van Allen, et al., "Energetic Electrons in the Magnetosphere of Jupiter," p. 309; J. H. Trainor, et al., "Energetic Particle Population in the Jovian Magnetosphere: A Preliminary Note," p. 311; R. W. Fillius and C. E. McIlwain, "Radiation Belts of Jupiter," p. 314.

22. Divine, T. N., "Interplanetary Charged Particle Environments," Technical Memorandum 33-637, Jet Propulsion Laboratory, Pasadena, California, August 1, 1973.

23. Horne, W. E. "Literature Search and Radiation Study on Electronic Parts Final Report," The Boeing Company, D2-126203-3, May 1970.

24. Brucker, G. J., "Sensitivity of Silicon Imaging Devices to Radiation on Missions to Jupiter and the Outer Planets," IEEE NS-19 No. 6, 1972. Also, Brucker, G. J., Final Report to JPL, same title.

25. Parker, R. H., "Effects of Proton Irradiation on Several Spacecraft Science Components," IEEE NS-19, No. 6, p. 156, 1972.

26. Barengoltz, J. B., "Jupiter Radiation Test Levels and Their Expected Impact on an Encounter Mission," Proceedings of the National Symposium on Natural and Manmade Radiation in Space, E. A. Warman, ed., NASA TMX-2440, p. 781, 1972.

27. Danchenko, V., "Radiation Damage in MOS Integrated Circuits, Part 1," X-711-71-410, Goddard Space Flight Center, Greenbelt, Maryland, September 1971.

28. Aubuchon, K. G., IEEE Trans. Nuc. Sci. NS-18, 117 (1971).

29. Hughes, H. L., IEEE Trans. Rel. Physics Sym., IEEE Catalog 71-C-9-ply 33, 1971.

30. Hughes, H. L., R. D. Baxter, and B. Phillips, IEEE Trans. Nucl. Sci., Dec. 1972, Volume NS-19, No. 6, p. 256.

31. Peel, J. L., and G. Kinoshita, IEEE Trans. Nucl. Sci., Dec. 1972. Volume NS-19, No. 6, p. 256.

32. Schlesier, K. M., and P. E. Norris, IEEE Trans. Nucl. Sci., Dec. 1972, Volume NS-19, No. 6, p. 256.

33. Barengoltz, J. B., JPL, Private communication.

NASA — JPL — Coml., L.A., Calif.